Hydrodynamic modelling approaches to assess mechanisms affecting the structural performance and maintenance of vortex drops shaft structures

Alan Carty[a], Colin O' Neill[a], Stephen Nash[ab], Eoghan Clifford[ab] and Sean Mulligan[ab]

[a]College of Engineering and Informatics, National University of Ireland Galway, University Road, Galway, Ireland ; [b]Ryan Institute, National University of Ireland Galway, University Road, Galway, Ireland

Alan Carty, College of Engineering and Informatics, National University of Ireland Galway, University Road, Galway, Ireland, email: alan.carty@nuigalway.ie

Hydrodynamic modelling approaches to assess mechanisms affecting the structural performance and maintenance of vortex drops shaft structures

Vortex drop shafts, a key hydraulic structure within modern day deep sewer conveyance systems, must be designed structurally to sustain performance and longevity of operating life under very energetic loading conditions. This has significant cost implications but to date little research has been undertaken to investigate the loading conditions with a view to optimising the shaft designs and thus lowering costs. In this study, several modelling methods were adopted to simulate hydrodynamic conditions within a vortex drop shaft to assess hydrodynamic mechanisms that impact a drop shaft liners structural performance and maintenance. A 1/10 scaled physical hydraulic model of a tangential inlet vortex drop shaft structure is tested and used to validate a three-dimensional multiphase numerical model. Collectively, the study presents methods on identifying hydrodynamic phenomena such as pressures, velocities, erosion and abrasion mechanisms, debris impact locations and blocking mechanisms. The study highlighted that the hydrodynamic forces that threaten structural integrity reside in the vortex generator and a short length of the drop shaft downstream. This is shown through a new model developed by the authors to predict centrifugal forces along the length of the drop. Through these methods, the study proposes that drop shaft liners can be designed more efficiently.

Keywords: vortex, drop shaft, drop shaft liners, deep tunnel conveyance, sewers, hydraulic structures

Introduction

Over the past 30 years, existing sewer infrastructure upgrade programs have seen the construction of deep tunnel conveyance and storage systems to help control storm weather overflows from combined sewers in urban areas worldwide (Schultz et al, 2004). A major challenge of such systems is the safe and efficient conveyance of combined sewer flows from existing wastewater networks down to lower tunnel levels through extensive elevation differences which can be as great as 170 m (Jain and Kennedy, 1983; Tai et al, 2009; Williamson, 2001, Vischer and Hager, 1995; Plant and Crawford, 2016). Vortex drop shafts (Figure 1) are efficient, low horizontal footprint devices with a proven record in wastewater

engineering applications (Plant et al, 2016, Hager, 1985; Williamson, 2001). They operate by conveying flow tangentially into a vortex chamber to generate a free-surface vortex flow. The diameter of the vortex air core first decreases and then increases from the generator to the vertical drop shaft which forms a throat at the contracted section. The free-surface is not uniform within this region due to the tangential inlet and thus the air core does not maintain centrality or verticality (Chen et al., 2010). As the flow discharges axially from the vortex generator into the drop shaft, the residual centrifugal forces in the flow combined with the Coanda effect (Weiss et al., 2010; Vischer and Hager, 1995) cause the water to cling to the walls of the shaft on its transition to the bottom stilling basin (Weiss et al., 2010). This longer helicoidal path that the fluid takes along the walls induces energy dissipation through friction and aeration (Hager, 1990; Jeanpierre and Lachal, 1966).

In terms of operation, vortex drop structures are generally considered superior to other drop structures such as plunge-flow drop shafts given that (1) they maintain a stable flow pattern for various discharges and (2) energy dissipation is enhanced through the vortex flow mechanics (Williamson, 2001; Rhee et al., 2018). For example, Vischer and Hager (1995) reported a 170 m high vortex drop shaft in Curbans, Italy developed for a design discharge of 140 m^3/s, while in China, a vortex drop shaft for the Shapai hydropower Station was designed with a drop height of approximately 100 m and a design discharge over 200 m^3/s (Dong and Gao, 1995).

Apart from efficient energy dissipation, vortex drop shafts provide several other advantages including accurate monitoring of flow by depth measurement, stable air core generation for natural venting, self-limiting operation, minimal risk of blockage and allow for non-uniform approach flow conditions. In terms of maintenance, drop structures are designed to be as maintenance-free as possible; in some cases, it is the upstream or downstream

appurtenances such as flow gates, monitoring equipment or trash racks that necessitate regular maintenance (Williamson, 2001).

Vortex drop shafts comprise three main elements (see Figure 1): an inlet structure, the drop shaft and the outlet structure. The inlet structure is responsible for producing the initial swirling flow as described by Jain and Ettama, (1987) and Mulligan et al., (2016) and typical inlet configurations include the spiral or scroll (subcritical inlet) inlet (Hager, 1990; Mulligan et al, 2016, Mulligan et al., 2018a, Rhee et al., 2018), tangential (supercritical inlet) (Jain, 1984) and slot vortex inlet (Quick, 1990). On the other hand, the outlet structure aims to safely dissipate the remaining energy in a stilling basin and direct an almost vertical annular jet to a horizontal conduit to deaerate the air–water mixture (Vischer and Hager, 1995). Regardless of the type of inlet structure, the flow processes are generally similar in vertical shafts and energy dissipation in the shaft is expected to be of the order of 90% (Jain and Kennedy, 1984). As the flow transitions through the shaft, air mixes with the flow and tremendous forces can be generated, resulting in a variety of hydraulic and structural design issues. Destructive pressure surges, impact damage due to debris and particle laden sewer flows and increased wear through abrasion on structures are some of the key processes that threaten the structural integrity of the vortex drop shaft if not properly considered during the modelling and design stage (Plant and Crawford, 2016; Williamson, 2001).

(a)

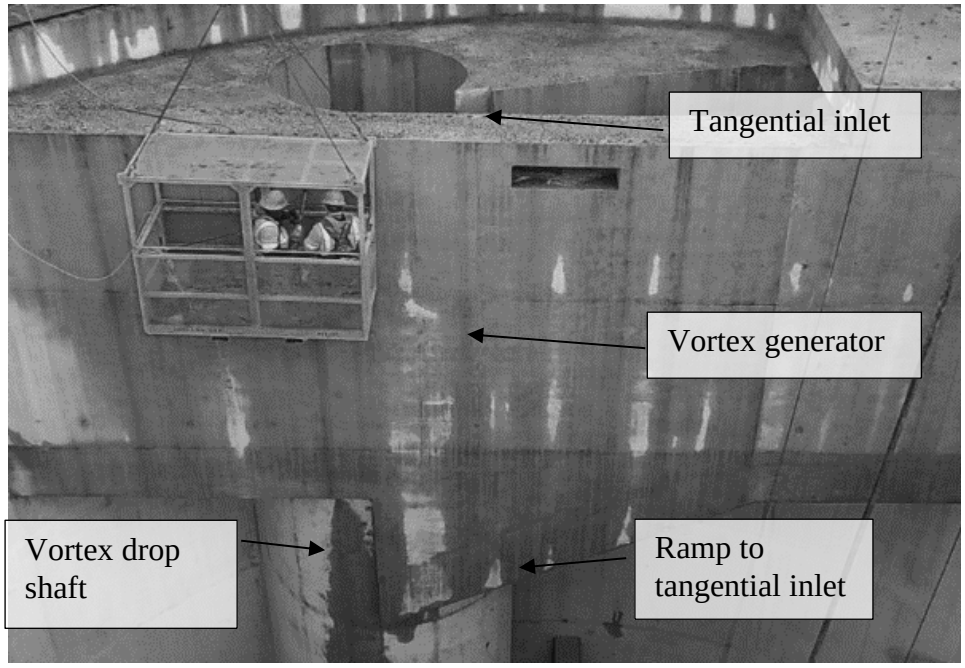

(b)

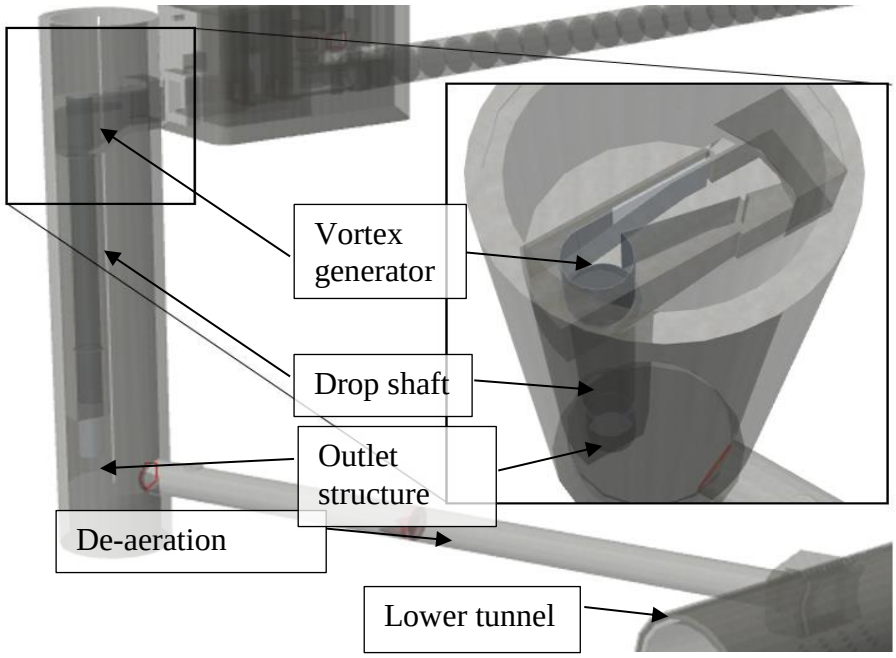

Figure 1. (a) Supercritical vortex drop shaft in the Main Pumping Station Diversions Project, District of Columbia (Image courtesy of District of Columbia Water and Sewer Authority) and (b) overview of the vortex drop shaft structure (Image courtesy of Ward and Burke Construction Ltd).

Numerous physical modelling studies have been carried out on the supercritical approach flow type vortex chambers (Plant and Crawford, 2016; Yu and Lee, 2009; Jain, 1984; Kellenberger, 1988; Motzet and Valentin, 2002). In contrast to physical modelling, only a few

93 studies have been undertaken on vortex drop shafts using numerical methods (Škerlavaj et al.,
94 2014; Mulligan, 2015; Kim et al., 2014; Plant and Crawford, 2016). Experimental studies on
95 vortex drop shafts have mostly focused on site-specific geometries in the context of the design
96 of commercial projects (Jain and Kennedy, 2983; Laushey, 1953). Only a few of these studies
97 investigated mechanisms responsible for structural degradation or failure. For example,
98 Anderson and Dahlin, (1975) have explored (via physical modelling) the effects of impact and
99 scour and various devices have been employed to determine the most effective and economical
100 means of dissipating flow energy. In these studies (Anderson and Dahlin, 1975; Dahlin and
101 Wetzel, 1985; Anderson, 1961) pressure fluctuations and energy spectrums in the outlet
102 structure stilling basin was primarily of interest where the authors made use of pressure
103 transducers or load cells in the model. High spikes indicating high energy dissipation at a
104 discrete frequency could cause damage to the prototype structure if this spike occurred at the
105 natural frequency of the structure (Anderson and Dahlin, 1975).

106 Alongside the stilling basin, knowledge of fluid structure interaction within the vortex
107 generator and drop shaft is key to informing suitable and economical material choice for the
108 drop shaft liner. In general, the pressure forces acting on most of the liner can be said to be
109 small when the annular jet thickness t_j is small (Jain 1987) and the velocity in the jet is
110 primarily axial. However, as described by Zhao et al., (2006) the pressure force could be
111 important when the water thickness varies quickly such as in the vortex generator. As far as
112 the authors are aware, there has so far been no experimental or numerical (hybrid) studies
113 undertaken to investigate the fluid structural interaction in this region of the hydraulic structure
114 where higher levels of knowledge on the underlying hydraulics may aid in progressing
115 economic design as opposed to over-engineered structural solutions.

116 In terms of material choice, Williamson (2001) describes a wide variety of material
117 linings, plastic membranes, coatings and other materials to maximize longevity against impact,

erosion and corrosion where durability, maintenance, constructability and cost are considered for the appropriate selection of materials. Recently, high structural and corrosive resistance design capacity materials such as stainless steel has been the material choice for the full extent of the drop shaft (Stayton, 2017; UK Water Projects, 2015). This is most likely for the purpose of conservatism in the absence of a proper understanding of the fluid structure interaction in the vortex liner system. With the vortex generator only constituting a small portion of the overall drop shaft structure, the question is posed as to whether high structural design capacity materials are necessary for the full extent of the structure. Thus, the argument in this study put forward is, through an enhanced understanding of hydrodynamics in the vortex drop shaft, can the hydraulic structure be designed and constructed more economically without compromising structural longevity?

In this article, an experimental and numerical (hybrid) study was undertaken to investigate the hydrodynamic flow processes and mechanisms that influence structural performance of the vortex drop shaft liner. In particular, the focus of the study is to consider the transition from the linear approach flow in the upper sewer system to the annular jet flow in the downstream drop shaft and consider the driving mechanisms that influence design. Physical modelling was used to investigate the general hydraulic behavior, track streamline projections in the generator to consider the dominance of centrifugal and axial forces, identify locations prone to impact by debris within the flow, resolve critical free-surface characteristics and to determine pressure fluctuations acting on the drop shaft liner. This physical data was also used to validate a three-dimensional numerical model of the hydraulic structure from the generator to the drop shaft outlet and consider global pressures and forces acting on the structure. Comments with regards to maintenance of the hydraulic structure are also outlined following highly conservative debris blocking scenarios. All modelling and analysis was undertaken on a 1/10 scaled model of a tangential inlet vortex drop shaft.

Theory and Operation

At the inlet to the hydraulic structure, the water is conveyed from the existing sewer or culvert via a rectangular open channel of width B and an approach flow depth h. As the flow rate Q is conveyed down the ramp of slope S, the approach flow channel begins to narrow towards a throat width of b before entering the vortex generator. The kinetic energy of the water increases as it accelerates down the channel, and a further increase in the velocity due to a decrease of cross-sectional area converts the available potential energy largely into kinetic energy at the inlet which is available to initiate a strong vortex flow. Due to the combined effects of the ramp and the converging inlet, the fluid entrance velocity has two major components described through the polar coordinate system θ, r, Z as outlined in Figure 2; the tangential (angular) velocity v_θ and the downwards axial velocity v_z. The third, radial velocity component v_r can be assumed to be negligible (Zhao et al., 2006). The resulting velocity vector V at the inlet can be resolved through continuity from Q/bh (Mulligan et al, 2016; Ackers and Crump, 1960) and from this, $v_\theta = Q/bhCosS$ and $v_z = Q/bhSinS$ where S (assuming that the angle of the mean flow velocity at the inlet approximates closely to the inlet ramp slope S). v_θ plays a crucial role in generating centrifugal forces through ${v_\theta}^2/r_{in}$ (where r_{in} is the inlet radius or expressed as the drop shaft diameter by $r_{in} = D/2$ for friction energy dissipation in the chamber. The vortex strength is then governed by the bulk circulation $\Gamma_\infty = 2\pi r v_\theta$. In many studies, the vortex is assumed to be fully irrotational such that the circulation is constant and thus the tangential velocity v_θ at radius r can be resolved through $v_\theta = \Gamma_\infty/2\pi r$ (Yu and Lee, 2009; Zhao et al., 2006).

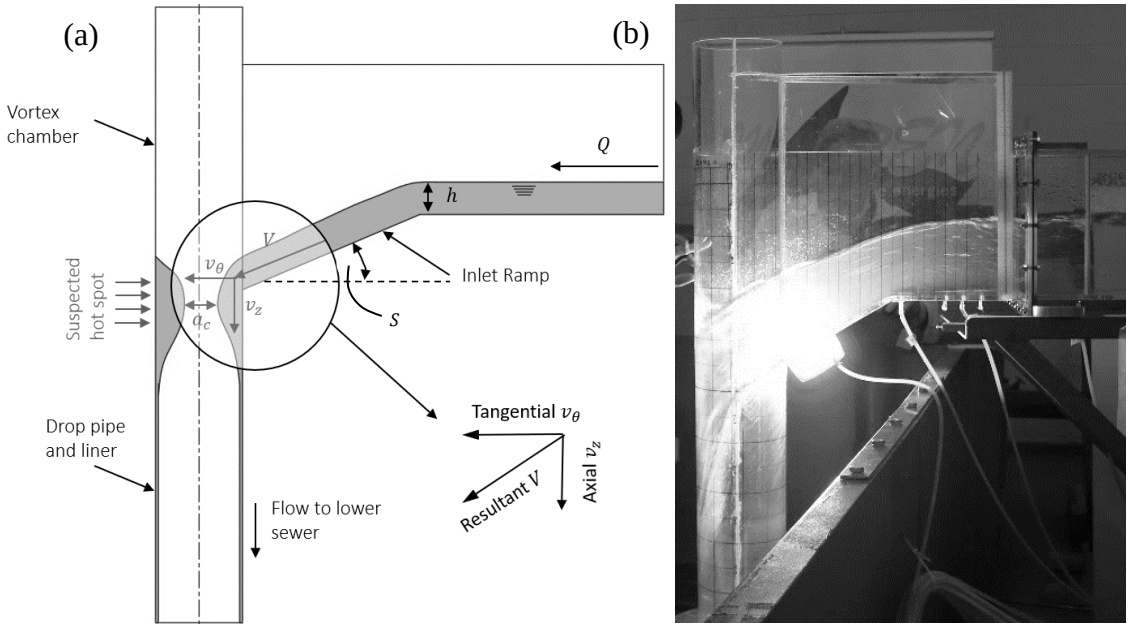

Figure 2: (a) Cross sectional schematic of the flow domain outlining the interaction between the major hydraulic parameters and the hydraulic structure and (b) physical model of approach flow channel and vortex generator

Physical Hydraulic Modelling

Hydraulic Similitude

In prototype sewer hydraulic structures, the tunnels, culverts and shafts will most likely be empty at the beginning of a storm event and will fill gradually reaching maximum capacity during extreme storm events. In other events, a full flow can be reached almost instantaneously due to the opening of a sluice gate or other processes putting additional shock stresses on hydraulic structures. In this study, model investigations of a scaled vortex drop shaft at 1/10 scale were explored for the full range of flows typically expected in such a sewer project. In both the prototype and the model, gravity is the predominant force governing hydraulic conditions. Thus, the greatest degree of dynamic similarity is when Froude similitude is maintained between the model and prototype. The scaling factors outlined in Table 1 were developed based on Froude similitude for the geometric length ratio $\lambda = L_p/L_m$ = 10.

Table 1. Scaling laws based on Froude similitude

Variable	Dimensions	Unit	Scaling Law
Length	L	L	$L_p = \lambda L_m = 10L_m$
Time	T	T	$T_p = \lambda^{1/2} T_m = 3.16T_m$
Velocity	V	LT^{-1}	$V_p = \lambda^{1/2} V_m = 3.16V_m$
Acceleration	A	LT^{-2}	$A_p = A_m$
Discharge	Q	L^3T^{-1}	$Q_p = \lambda^{5/2} Q_m = 316.22V_m$
Force	F	MLT^{-2}	$F_p = \frac{F_m}{\lambda^{1/2}} = 0.316F_m$
Pressure	P	ML^2T^{-3}	$P_p = \lambda P_m = 10P_m$
Mass	M	M	$M_p = \lambda^3 M_m = 1000M_m$

As a result of obeying Froude similitude alone, there is a likelihood for scale effects to also be entrained in the model as a consequence of neglecting the effects of surface tension and viscosity; characterised by the Weber number and Reynolds number respectively. Flow characteristics and energy dissipation are however said to be properly simulated in a Froude model once the flow is sufficiently turbulent. For vortex drop shafts it is necessary to achieve $\mathrm{Re} > 10^5$ (Zielinski and Villemonte,1968) and $\mathrm{We} > 120$ (Jain et al., 1978). In the current study, the minimum model Reynolds and Weber numbers in the vortex drop shaft were found to be above these limits.

Hydraulic Model and Test Rig

The physical model had shaft diameter of $D = 168$ mm and was constructed from 6 mm transparent acrylic, see Figure 2 (a) and (b). The model was installed on an existing sewer model test rig which comprises of a 4 m^3 water storage tank and 100 mm uPVC pipe system, seen in Figure 3. Flow was pumped through the system with a range of between 0 to 30 l/s which was controllable using a variable speed drive and monitored using electromagnetic flow meters which have a max reading error of ± 0.2 % and a reading standard deviation of ± 0.006

l/s. Water levels were extracted from the planar acrylic surface of the approach flow. A 0 to 2 PSI (0 to 1.4 m head of water) pressure transducer (Omega PX309-002GV) with a 3.25 % error (determined during calibration) was installed horizontally at two locations in the drop shaft, (1) located at 50 mm above the ramp insertion point to the drop shaft, where the focused inlet jet impacts in the vortex generator and (2) 300 mm downstream of the ramp insertion point of the vortex generator to monitor pressure fluctuations in both regions respectively, as seen in Figure 4. Pressure readings were monitored at 50 Hz for one minute using Instrunet World. The hydraulic grade line was accessible along the channel invert approaching the drop shaft using manometer tapings. For all investigations, steady flowrates of $Q = 3.6$, 6.5, 13.3, 18.0, 21.6 and 24 l/s were investigated. The selection of Q was based on scaled flow conditions that were to be expected on a live hydraulic structure, which were tested in another project.

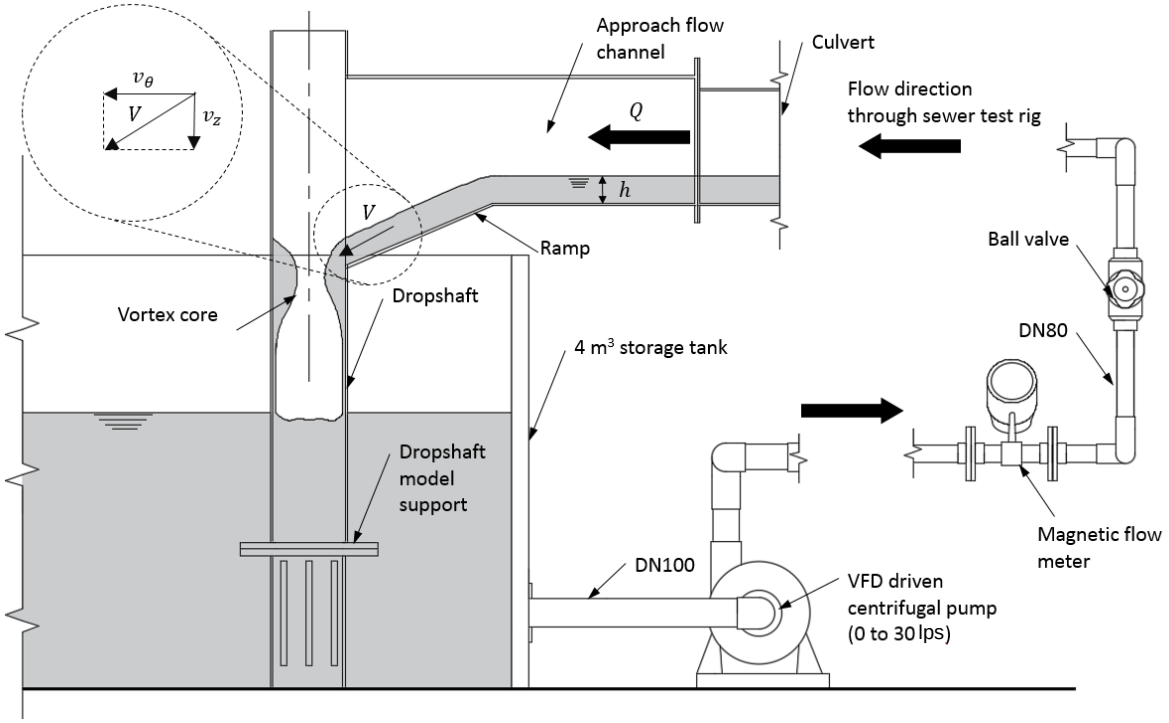

Figure 3. Schematic of the test rig configuration outlining flow circulation and major instrumentation

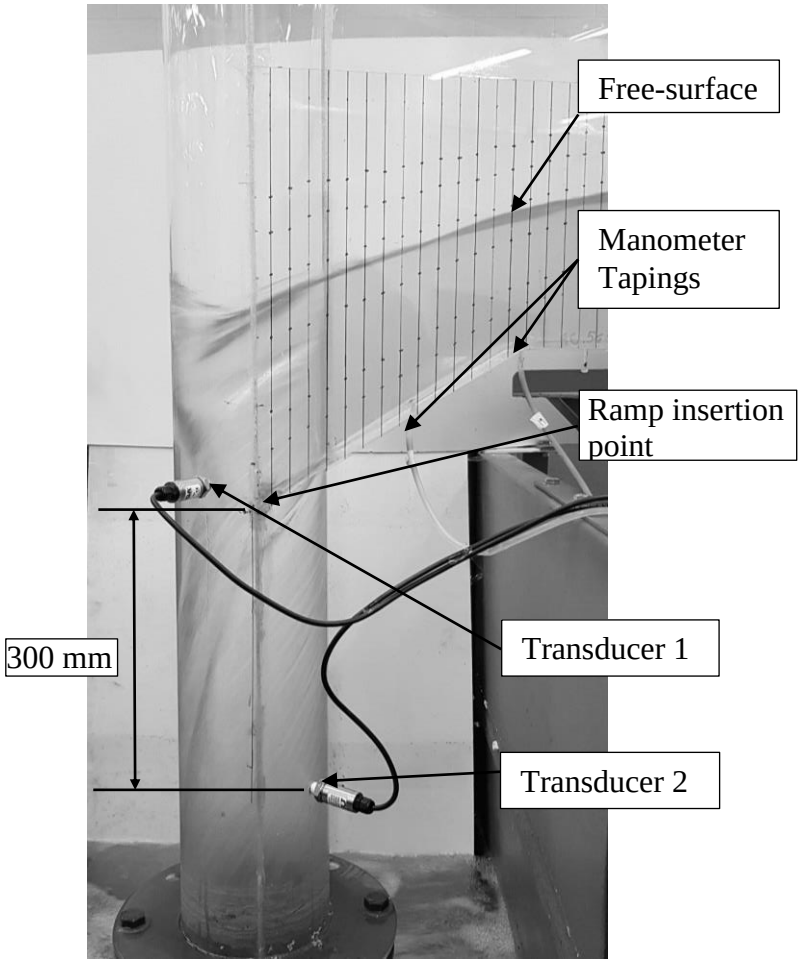

Figure 4. Image of vortex generator and initial portion of drop shaft outlining the position of pressure transducers and manometer tapings

Streamline and Debris Impact Analysis

Through the use of streamline tracing it was possible to visualise the trajectory of the mean fluid patterns as its transitions into the drop shaft. In the physical model, the streamlines manifest as stable and lightly aerated flow lines which were easily visualised when illuminated using an LED light as shown in Figure 5 (a). A circumferentially segmented chart made from and acetate sheet was used to shroud the shaft wherein the streamlines could be isolated and tracked as shown in Figure 5(b). Each segment was divided in to 360°/4 sections circumferentially and 900mm split into 100 mm sections vertically along the $z-$axis. The extracted streamlines were subsequently used to decipher the projection of the streamlines or

the rate of change of the streamline angle α with vertical height Z ($d\alpha/dZ$) from the inlet throughout the drop shaft within each quadrant as seen in Figure 5(c).

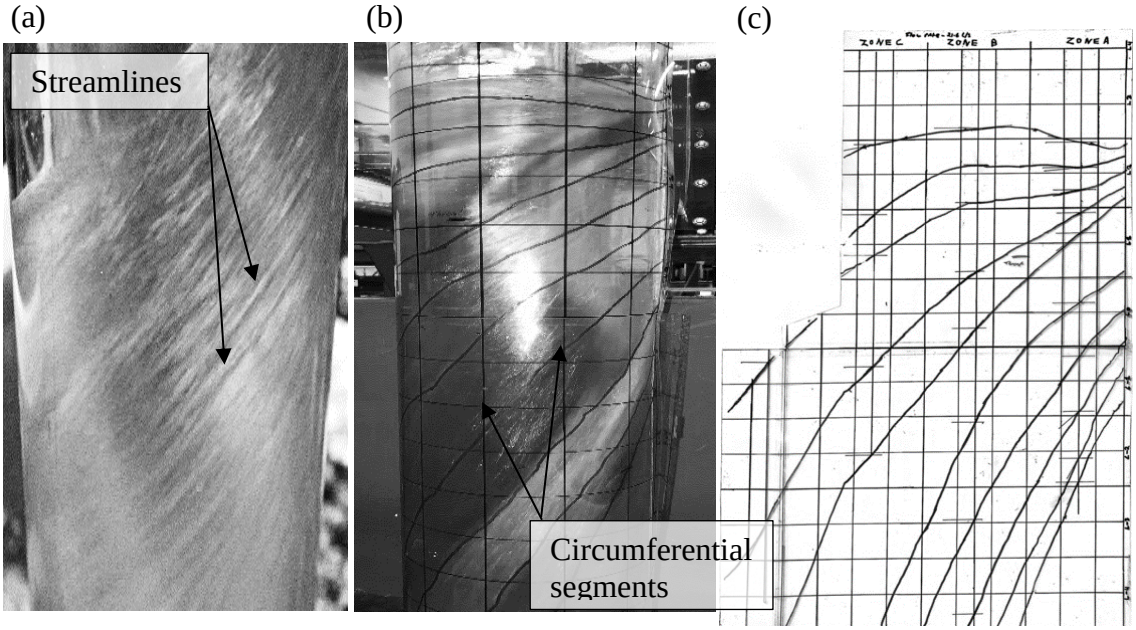

Figure 5: (a) Streamlines visible in drop shaft, (b) shrouding chart for extracting streamlines and (c) extracted streamlines spanning each quadrant indicating the relationship between axial and centrifugal forces in a drop shaft up to 500mm below the inlet.

Debris tracking analysis

As debris enters the vortex generator approach flow, it accelerates and gains momentum. A change in direction of this momentum as a result of contact with the hydraulic structure can result in significant impact forces. In the vortex generator, this may be particularly concerning in the region of the inlet where the debris must undergo a significant change in direction at the shaft liner at the hot spot outlined in Figure 2 previously. Using the *Kinovea* tracking software (www.kinovea.org), the trajectory of debris could be resolved up to their point of impact with the drop shaft liner. In this analysis, scaled railway sleepers (270 mm x 13 mm x 26 mm) with a density of 900 kg/m^3 were observed in transit into the drop shaft as shown in Figure 6. A marker was placed on the leading edge of the sleeper to facilitate tracking and its trajectory could be extracted as seen in Figure 6 below. Six debris trajectories and impact points were determined per flowrate.

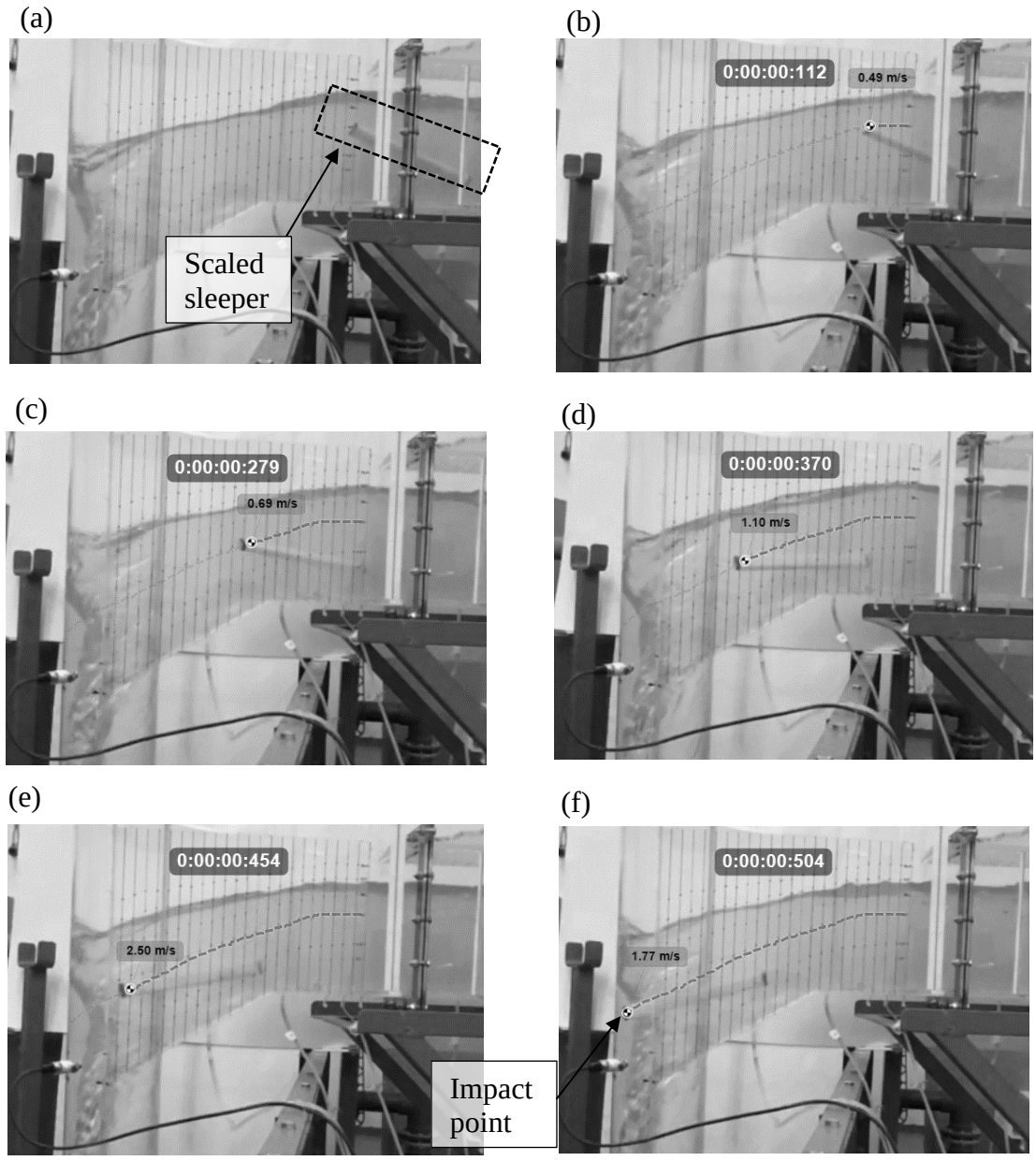

242 Figure 6: Debris tracking (a) initial entry and tracking at time-steps (b) t = 0:112 s, (c) t =
243 0:279 s, (d) t = 0:370 s, (e) t = 0:454 s, (f) t = 0:504s,

244 **Numerical Modelling**

245 Numerical modelling was performed using the commercial CFD software packages ANSYS
246 FLUENT (V19.0) and ANSYS CFX (V14.5). Both codes use different approaches to
247 discretising the Navier-Stokes equations (Wilcox, 1993). ANSYS CFX uses a hybrid finite-
248 element/finite-volume (finite element based finite volume method) whereas in contrast, the
249 ANSYS FLUENT solver uses finite volumes (cell centered numerics). Both CFD codes were

used to investigate the hydraulics of the vortex drop shaft following a CFD validation study which is described in detail by Mulligan et al., (2018b) and is described briefly here. The two-phase fluid domain was modelled using a homogeneous Eulerian-Eulerian multiphase flow model. This is a limiting case of the full Eulerian-Eulerian model which assumes that interphase momentum transfer is negligible and is valid for the current test case where the phases are completely stratified and the interface (free-surface) is well defined. In the homogenous approach, both phases are treated as interpenetrating continua parted by a well-defined interface and share common velocity, pressure and turbulence field. The tracking of the interface between the phases is accomplished by solving the volume fraction equation for one of the phases. For free-surface flows, this is based on the Volume of Fluid (VOF) method (Hirt and Nicholas, 1981).

Based on previous studies, it is recommended that for flows with strong rotation, the mesh should be aligned with the general flow pattern (Mulligan, 2015; Škerlavaj et al., 2014). As a result, a quasi-structured mesh was adopted as shown in Figure 7. This was achieved using an inflation layer with a first layer thickness of 0.5 mm which was also required to resolve the turbulent boundary layer. 6 mesh configurations were investigated as per Table 2 during the validation study to determine solution sensitivity to mesh density.

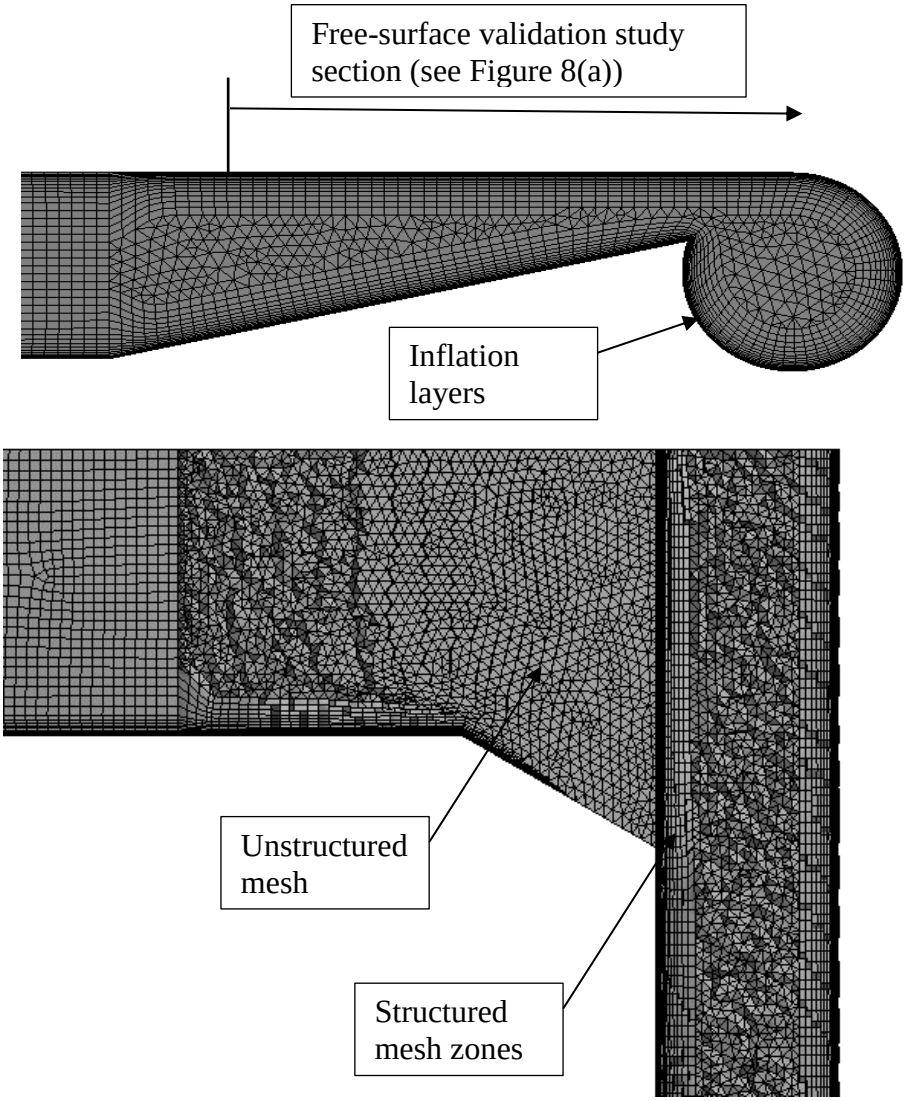

Figure 7: (a) Plan and (b) elevation of numerical mesh

Boundary Conditions and Test Cases

A mass flow or velocity at the inlet and a static pressure condition at the outlet utilised an opening with a zero-pressure boundary condition was imposed at the outlet and at the top of the structure. The walls were treated as no-slip smooth wall boundaries. Turbulence models are generally a modification of the unsteady Navier-Stokes equations by introduction of averaged and fluctuating quantities to yield the Reynolds Averaged Navier-Stokes (RANS) (Wilcox, 1993) equations. In this study, the key eddy viscosity turbulence models including the $k-\varepsilon$, shear stress transport (SST), SST with curvature correction (CC), transition SST four equation model were evaluated to assess the solution dependence on each accordingly.

Table 2: Phase 1 Sensitivity Study

#	Mesh Size (m) *	No. of Elements	Inlet Boundary Type	Turbulence Model	CFD Code
1	0.020	10,000	Fixed Head	k – ε	FLUENT
2	0.010	40,000	Fixed Head	k – ε	FLUENT
3	0.005	175,000	Fixed Head	k – ε	FLUENT
4	0.005	175,000	Fixed Head	SST	FLUENT
5	0.005	175,000	Fixed Head	SST-CC	FLUENT
6	0.005	175,000	Fixed Head	Transition SST	FLUENT
7	0.010	130,000	Fixed Head	k – ε	FLUENT
8	0.010	396,036	False Floor	SST	CFX
9	0.005	496,000	False Floor	SST	CFX
10	0.005	496,000	False Floor	SST-CC	CFX
11	0.005	496,000	False Floor	k – ε	CFX
* Mesh size is relative to the mesh size in the vortex drop shaft					

Numerical-Experimental Validation

In this section, the sensitivity of the numerical model and its accuracy in simulating the physical data is discussed with reference to the models tested in Table 2. Results from the free-surface and velocity were used for validation using the physical model. It's also important to mention here that modelling the drop shaft liner material was not undertaken as its effect in the model would have no bearing on the hydraulic behavior in the simulation. From this it is possible to show that the solution becomes more or less independent of the mesh when the number of elements exceeds 200,000. This corresponded to a drop shaft cell size of 5 mm (approximately 3 % of the drop shaft diameter). It was also found that significant errors can be introduced to the free-surface when inflation layers are omitted from the mesh structure. Table 3 presents the inlet velocity solutions (and error) for the various turbulence models. For the solution independent case it was found that the solution was not significantly reliant on the choice of turbulence model with relative errors falling below 9 %.

295 Table 3: Solution sensitivity to turbulence model

#	Code	Turbulence Model	Velocity (m/s)	Error (%)	No. of Elements
1	FLUENT	k-epsilon	1.162	20.41	10,000
2	FLUENT	k-epsilon	1.130	22.60	40,000
3	FLUENT	k-epsilon	1.335	8.56	175,000
4	FLUENT	k-epsilon	1.140	9.93	55,000
5	FLUENT	k-epsilon	1.380	10.27	130,000
6	FLUENT	SST	1.315	10.41	175,000
7	FLUENT	SST-CC	1.310	21.92	175,000
8	FLUENT	Transition SST	1.308	5.48	175,000
9	CFX	SST	1.580	8.22	396,036
10	CFX	SST	1.540	5.48	490,000
11	CFX	k-epsilon	1.500	2.74	490,000

- Velocity obtained at inlet to vortex generator b from continuity

296 Figure 8 (a) presents a comparison between the approach flow free surface for the physical,
297 FLUENT and CFX models. A good agreement can be observed between all of the models with
298 discrepancy (or model divergence) beyond 400 mm where the physical model water surface
299 rises due to the formation of a small hydraulic jump in the inlet throat. Figure 8(b) presents a
300 comparison between the physical and numerical (FLUENT) inlet velocity data for each
301 approach flow test case. The errors were found to be stronger for the low approach flows and
302 reduce to reasonable levels for flows greater than Q =10 l/s. This was attributed to effects of
303 surface tension (neglected in the numerical model) which may become influential for these
304 lower flow conditions where the Weber number We → 120 (Jain et al., 1978). Errors for lower
305 flow conditions may also originate from mesh resolution issues near the invert boundary
306 condition. Table 4 provides a qualitative comparison of all model results (physical, FLUENT
307 and CFX) where excellent agreements were observed in the free-surface position and shape,
308 including the jump observed beyond the inlet.
309

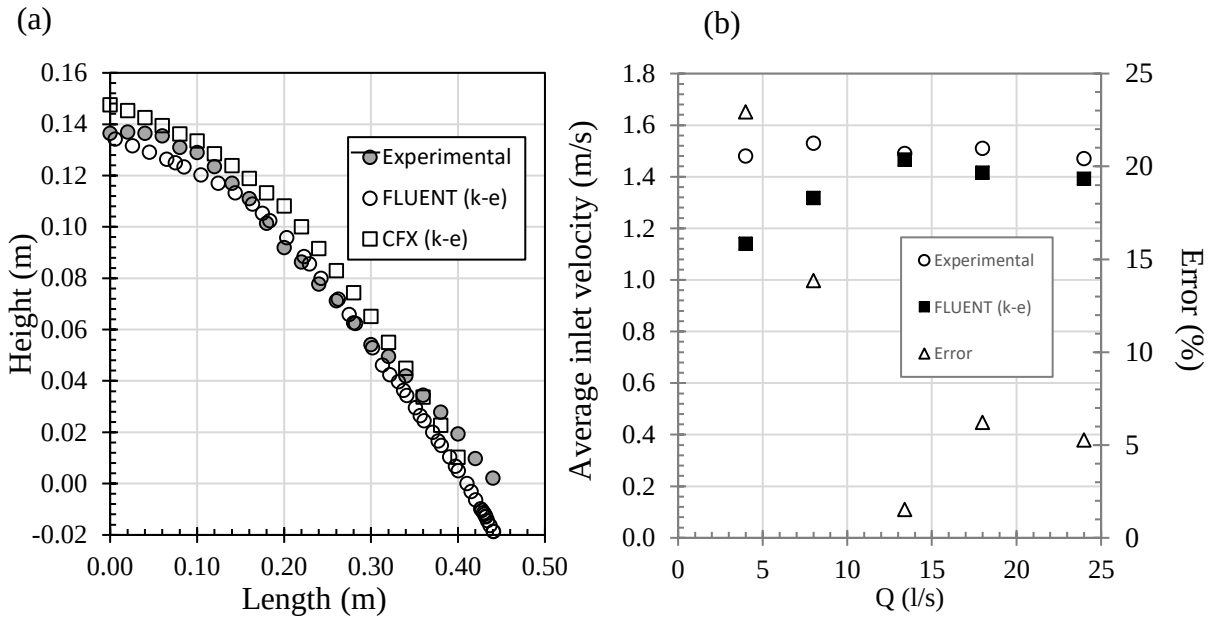

Figure 8. (a) Physical and numerical comparison of free-surface in the vortex generator approach flow channel and (b) error in predicting the average velocity at the inlet of the vortex generator

Table 4: Comparison between physical and numerical free-surfaces (FLUENT and CFX) for $Q = 4$ l/s, 8 l/s and 13.4 l/s (see Figure 9 for contour legend)

Flowrate Q (l/s)	Physical Model	FLUENT ($k-\varepsilon$)	CFX ($k-\varepsilon$)
4.0		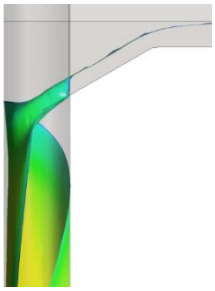	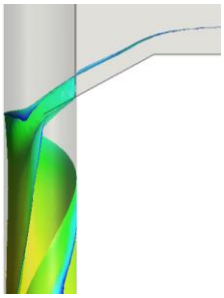
8.0		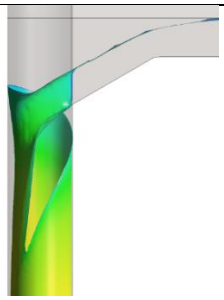	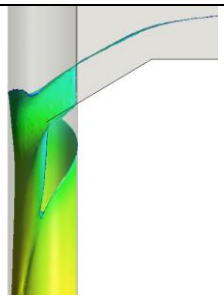
13.4		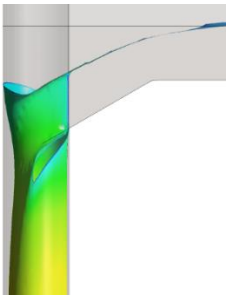	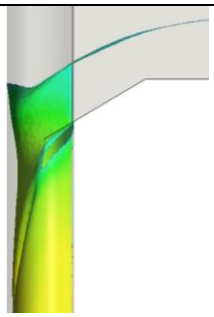

As discussed previously, the vortex air core and its stability is a principal aspect to be checked to ensure good performance of vortex drop shaft structures. Figure 9(a) presents a comparison between the physical model air core and the numerical simulation achieved with CFX where the shape and eccentric position of the core was well replicated. The transition between the free-drainage condition and inlet disturbance conditions was also well captured demonstrating that the numerical approach is a useful tool for identifying problematic stability conditions in the flow.

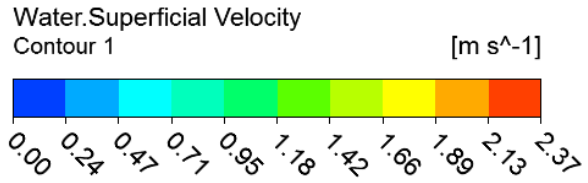

(a)

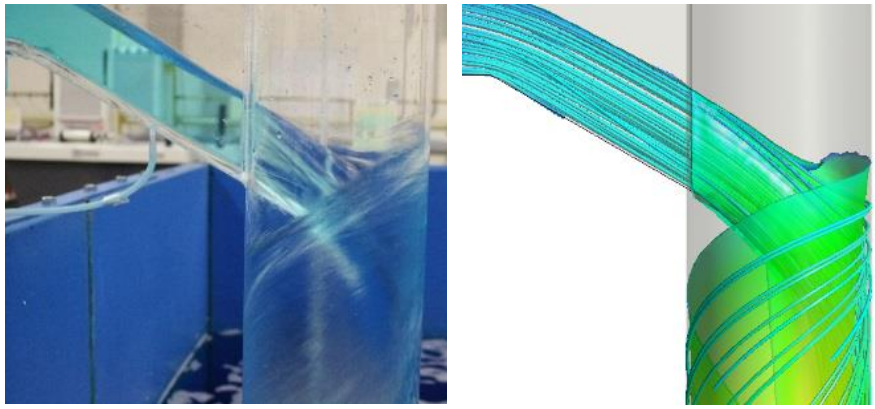

(b)

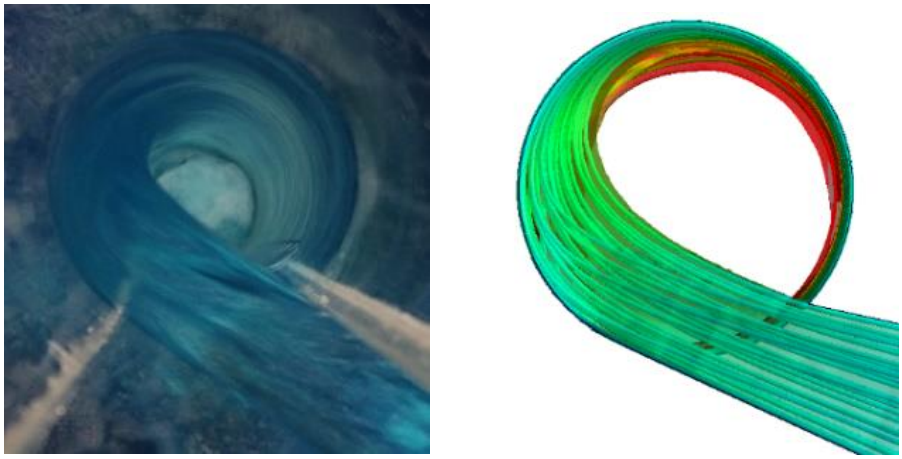

Figure 9. (a) Comparison of physical and numerical model for (a) inlet condition in the vortex generator highlighting a good prediction of the free-drainage discharge and (b) free-surface streamlines and asymmetric flow condition in the initial section of the drop shaft

Results

Air Core, Velocity and Pressure

Figure 10 shows the distribution of the air core and annular jet thickness t_j for various axial positions of the drop shaft Z. In the vortex generator, there is a rapid variation of air core circumferentially and vertically. As described by other studies, the air core is not

central or vertical in this region. The annular jet is more uniformly distributed below Z/D = 5 however still lacks complete symmetry in this region due to a steady helical wave that extends the full length of the drop shaft (see Figure 10 d, e and f).

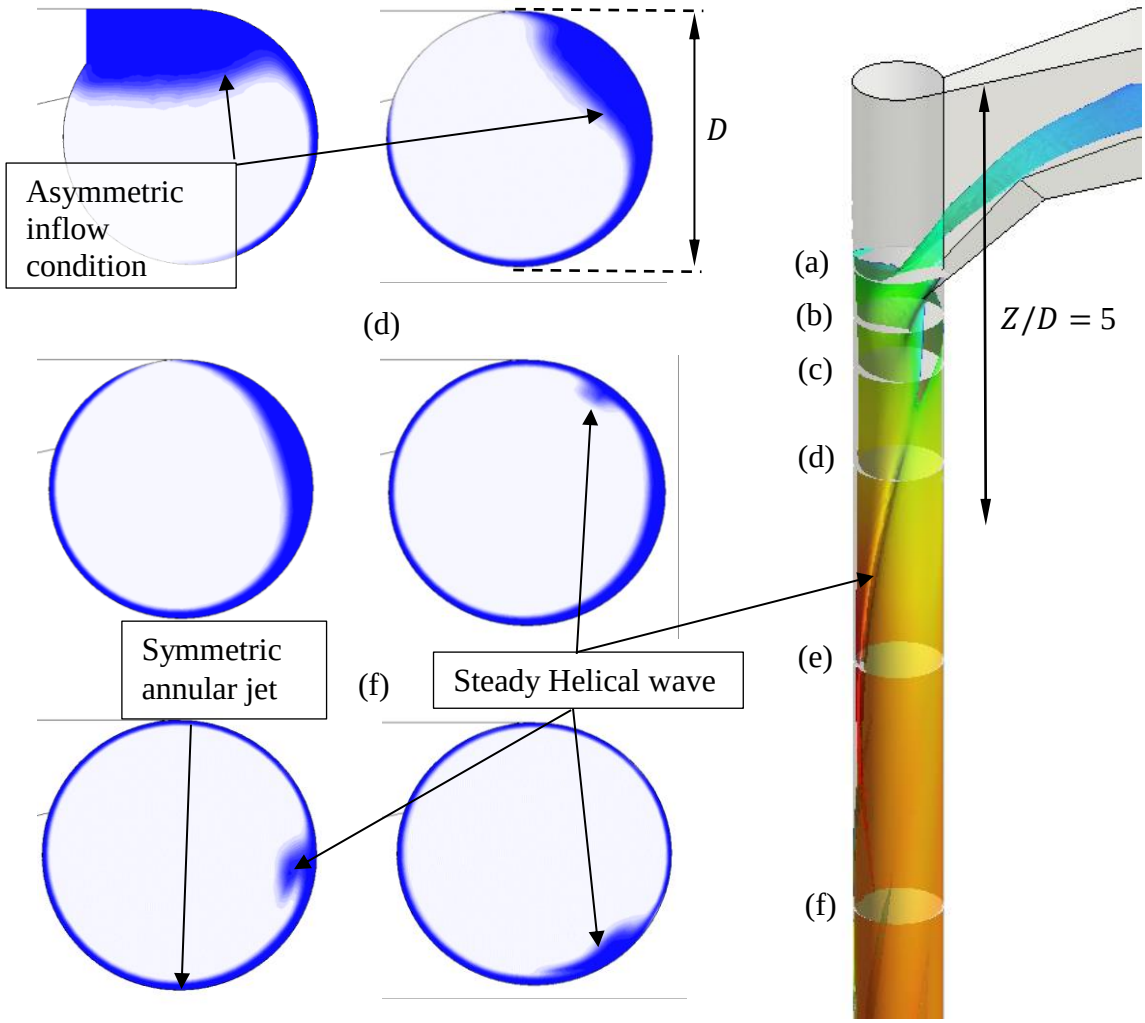

Figure 10. Air core characteristics axially in the vortex drop shaft for Q = 8 l/s highlighting asymmetric sections (a to c), largely axisymmetric annular flow (d to f) and the position of the steady helical wave (d to f)

Figure 11 presents velocity vector plots on the horizontal planes (a) and (b) (as highlighted din Figure 10) in the vortex generator. Once again, poor symmetry in the velocity distribution is depicted resulting from the tangential inlet. It can also be inferred from the velocity vectors that the tangential velocity distribution in the radial direction in the vortex drop shaft is largest near the drop shaft periphery and reduces close to the core

which infers that the velocity distribution follows that of a forced vortex (i.e. the circulation Γ is not constant in the vortex flow field as was assumed in past studies).

Figure 12 presents the axial distribution of tangential and axial velocity throughout the full extent of the vortex drop shaft for $Q = 8$ l/s. The tangential velocity is at a maximum in the vortex generator but is dissipated due to friction and converted to axial velocity as is depicted by the growth in the axial velocity from a minimum at the vortex generator to a maximum at its departure from the bottom of the drop shaft.

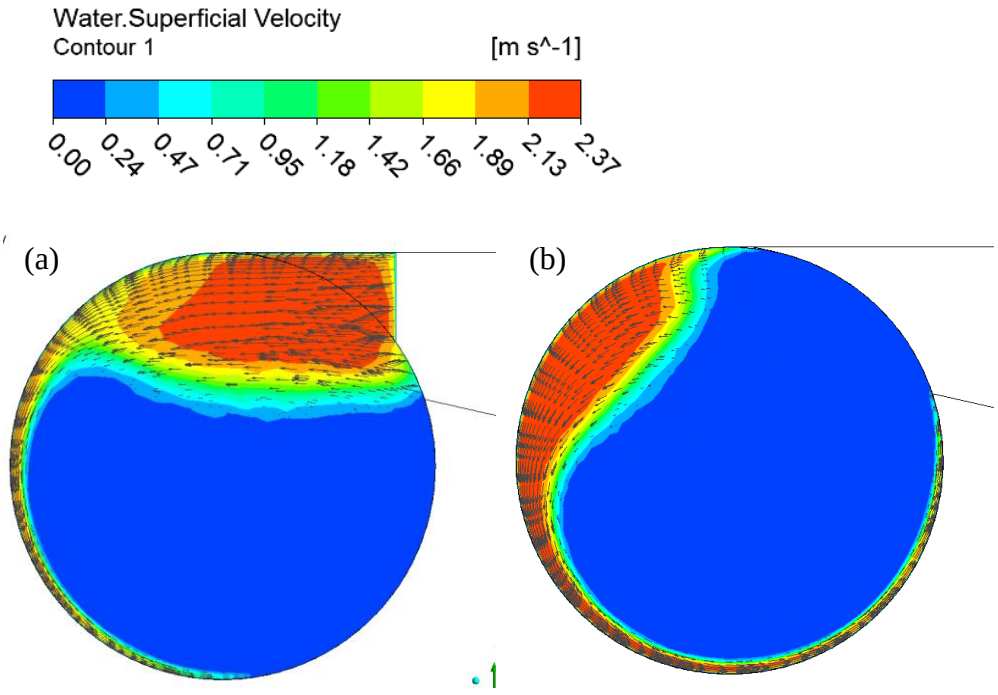

Figure 11. Velocity vector distribution for horizontal cross sections (a) and (b) in the vortex generator (refer to Figure 10) from CFX simulation

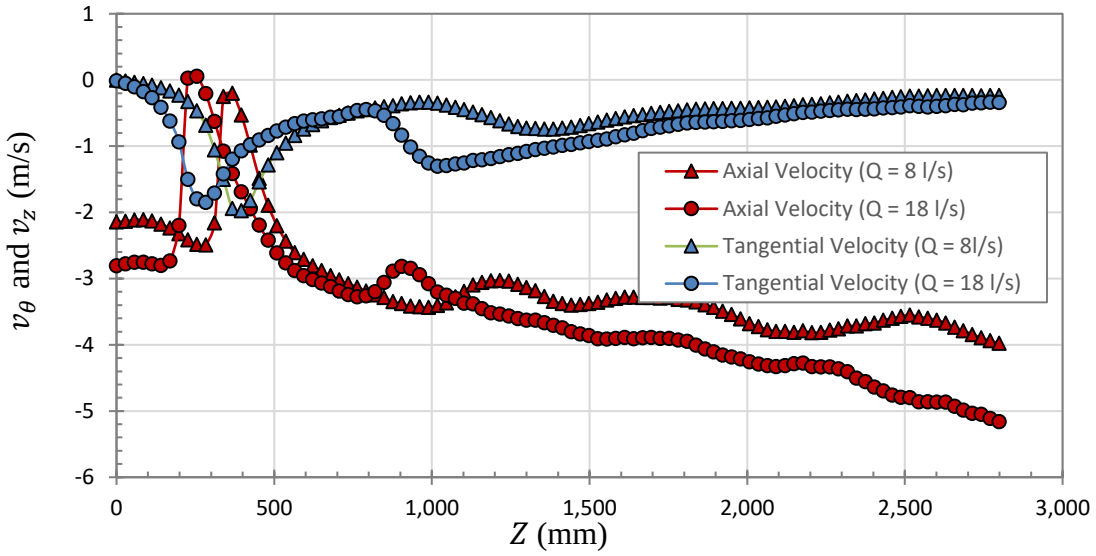

374

375 Figure 12. Tangential and axial velocity distributions axially in the vortex drop shaft
376 from CFX simulation

377 Figure 13 highlights that axial distribution of wall pressure along the drop shaft for $Q =$
378 8 l/s and 18 l/s. The peak pressures were experienced in the vortex generator region where
379 the tangential velocities were also at their maximum. This peak pressure increases as the
380 flow rate in the vortex generator is increased. The pressure appeared approaches zero (and
381 often sub atmospheric levels) when at a height of $Z/D = 5$ below the vortex generator.

382

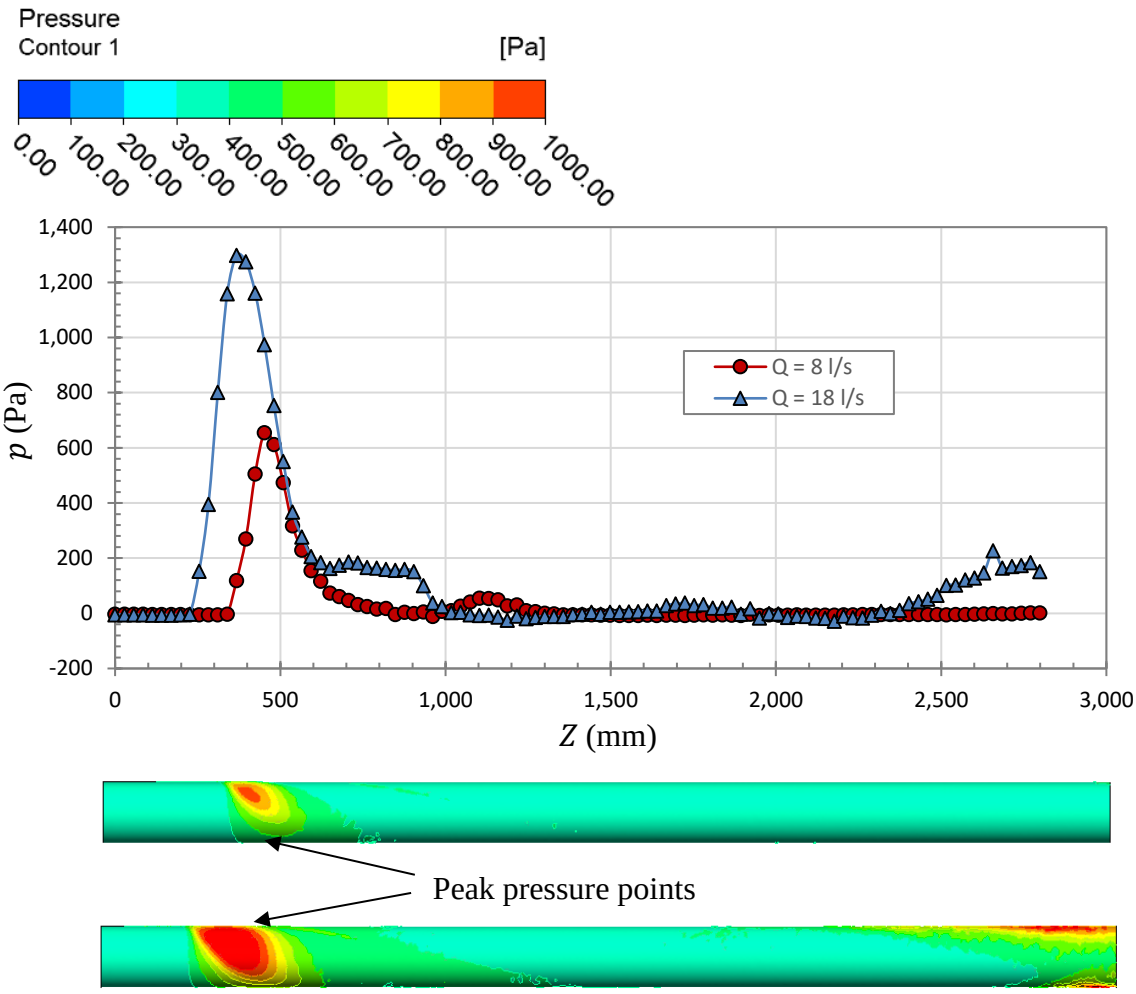

Figure 13. Time averaged CFX simulation results showing (a) Axial pressure distributions along the drop shaft liner for Q = 8 l/s and 18 l/s and pressure contours along the drop shaft liner for (a) Q = 8 l/s and (c) Q =18 l/s

The pressure fluctuations at the peak pressure zone were also monitored as described previously using a diaphragm pressure transducer. The one-minute time series of the pressure is presented in Figure 14 indicating the transient behaviour of the pressure in this region. The transient pressure wave varies from positive to negative values and exhibits frequencies of the order of 1.42 Hz and has variations between negative and positive pressures 8 kPa. The averaged pressure values are however positive and agree well with the numerical pressures resolved from ANSYS CFX and FLUENT.

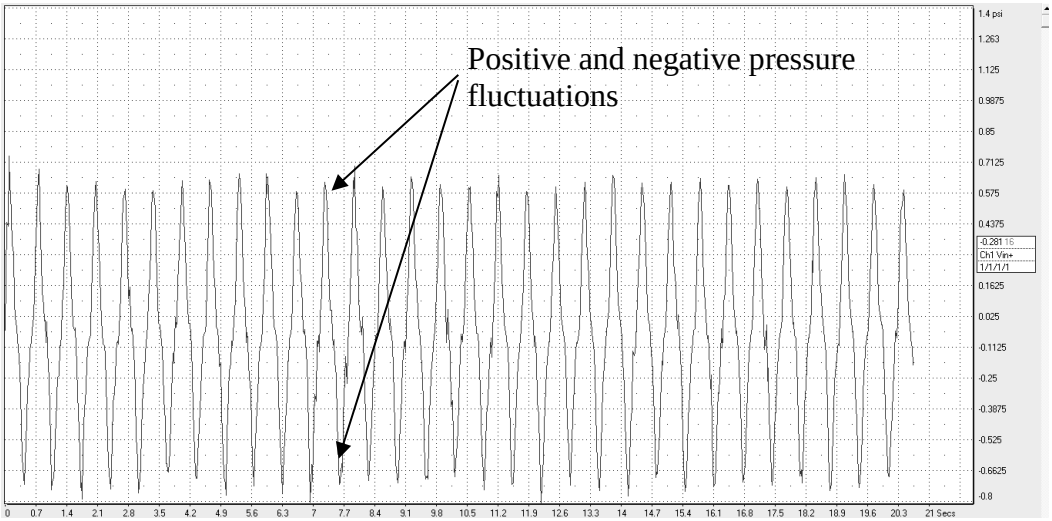

Figure 14. Pressure fluctuations on the drop shaft liner at the vortex generator inlet (Note, CFX pressure results were time averaged)

Streamline Analysis

It was initially observed in early stages of the streamline documentation that a definitive relationship was present between the axial and tangential angles. As can be seen in Figure 5 (b), Figure 5 (c) and Figure 15 that axial forces gradually overcome centrifugal forces, as the fluid transitions through the drop shaft it gravitates towards full axial flow. Zone A which denotes the first 90 degree turn through the vortex generator after the inlet experiences the highest circulation as is depicted by the slope of the blue line in each case.

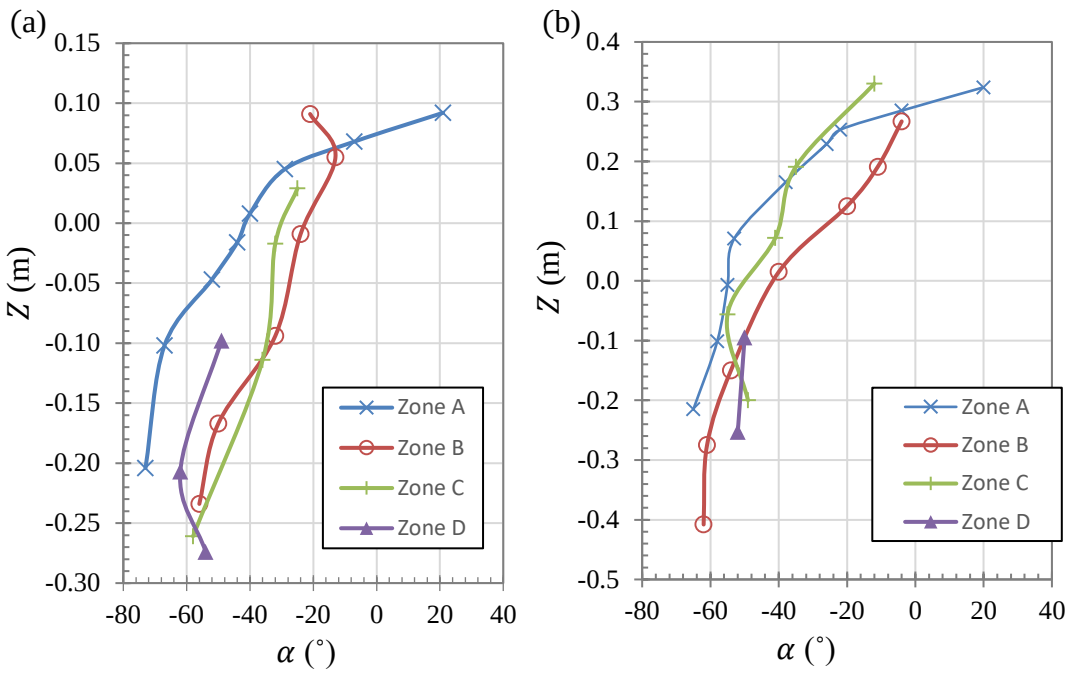

Figure 15. Relationships between streamline angle α and axial position Z for (a) Q =6.5 l/s and (b) Q =18.0 l/s

Debris Impact

Figure 16 highlights the relationship between resultant debris velocity and time for Q = 3.6 l/s and Q = 21.6 l/s as obtained from the debris tracking software. As the debris is initially transported in the approach flow channel, its velocity maintains relatively constant. At some position along the ramp (see Figure 1), the debris gains acceleration which is depicted by the slope in the graph for each case in Figure 16. The point of acceleration is different for each flow, initiating earlier for higher discharges. However, for each flow condition, the total acceleration of debris remains relatively constant at approximately 3.5 m/s^2. When the debris impacts the drop shaft liner, it appears to undergo a complete change in horizontal and vertical direction. Therefore, it can be assumed that the impact force of F_d = 0.266 N (266 N in the prototype) is generated on the drop shaft wall at each specific impact point from the mass and density of the sleeper (ρ =900 kg/m^3). This force can be resolved on the drop shaft liner as a force vector with

a horizontal component acting perpendicular to at a tangent to the point of impact. The vertical component can be resolved from the slope of the debris trajectory which was found to closely approximate the inlet slope angle S. The points of impact were resolved for 30 impact tests as is shown in Figure 17. It is apparent that the impact points are localised to a section within the first 90 degree (Zone A) turn of the vortex generator. The debris point of impact vertically is dependent on the flow discharge where for higher discharges, the impact points reside higher in the vortex generator.

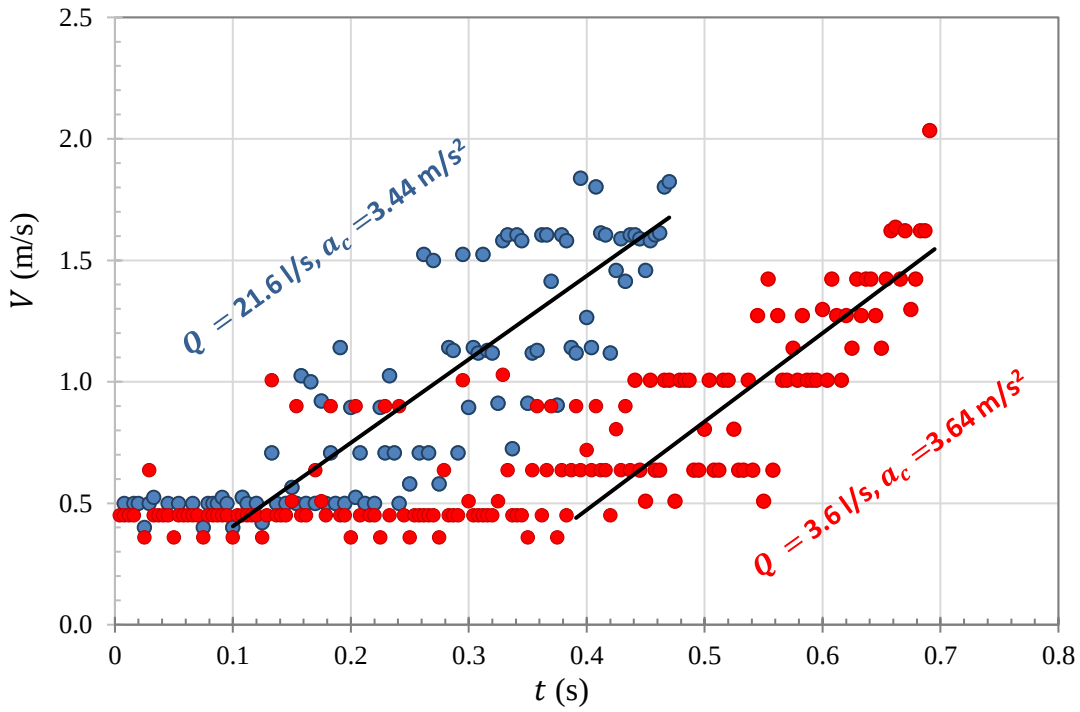

Figure 16. Relationship between debris resultant velocity and time as the debris is tracked on the approach to the vortex generator inlet (R^2 is 0.68 and 0.61 for 21.6 and 3.6 l/s respectively)

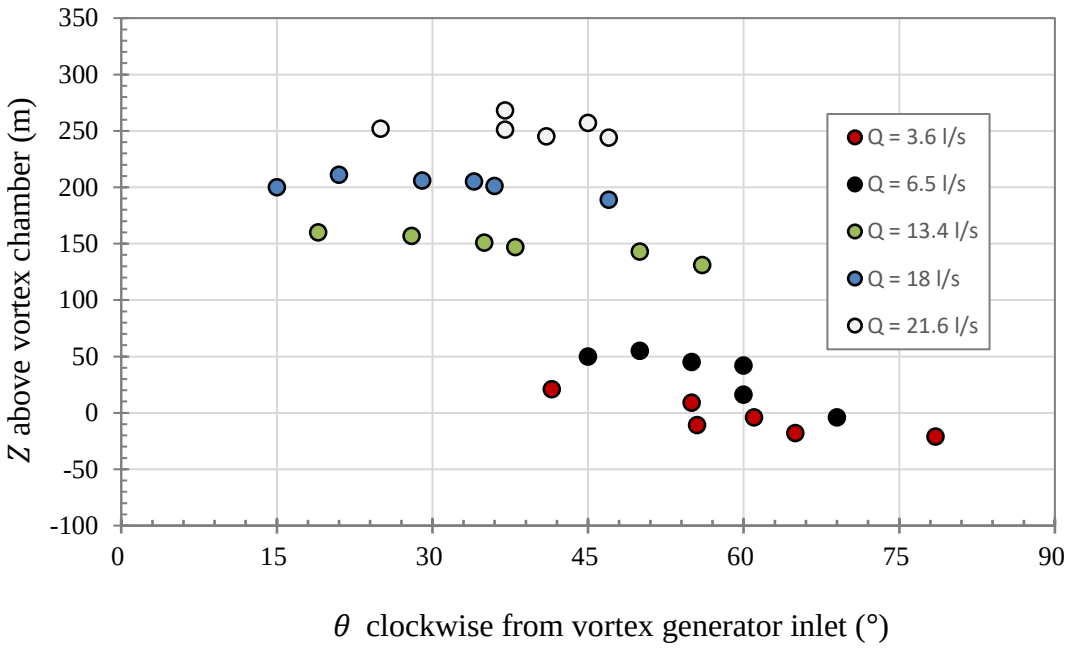

Figure 17. Debris impact locations in the first 90 degree turn of the vortex generator

Blocking Scenarios

Upstream of vortex drop shafts, it is often a case that there exist appurtenances which obstruct flow laden obstacles and debris. For example, it is known that debris can often accumulate in or behind flap valves and gates. Under the case where a large quantity of heavy debris is released abruptly from such appurtenances, they may be transported with the flow as a debris accumulation and cause issues downstream. As was shown previously, the vortex drop shaft is capable of passing relatively large debris such as railway sleepers in isolation. However, an experiment was conducted to observe the effect of two or more pieces of woody debris entering the vortex generator. This can be considered to be a highly conservative test given the probability of such an event occurring; however, the effect of such an event occurring is nonetheless a fruitful investigation. As can be observed in Figure 18, when two floating sleepers enter the vortex generator inlet, they become jammed in the narrow entry. The result is an increase in upstream head and hydraulic gradient which may cause problems upstream. However,

as can be seen in Figure 18, this issue also perturbs the downstream flow dynamics where the flow now cascades over the jammed sleepers (b) causing a drowning effect on the vortex flow and air core (d). Essentially the outcome is that the vortex drop shaft is converted into a form of plunge flow drop shaft which is worsened if more debris is to build up behind the jamming mechanism (see Figure 18(d)).

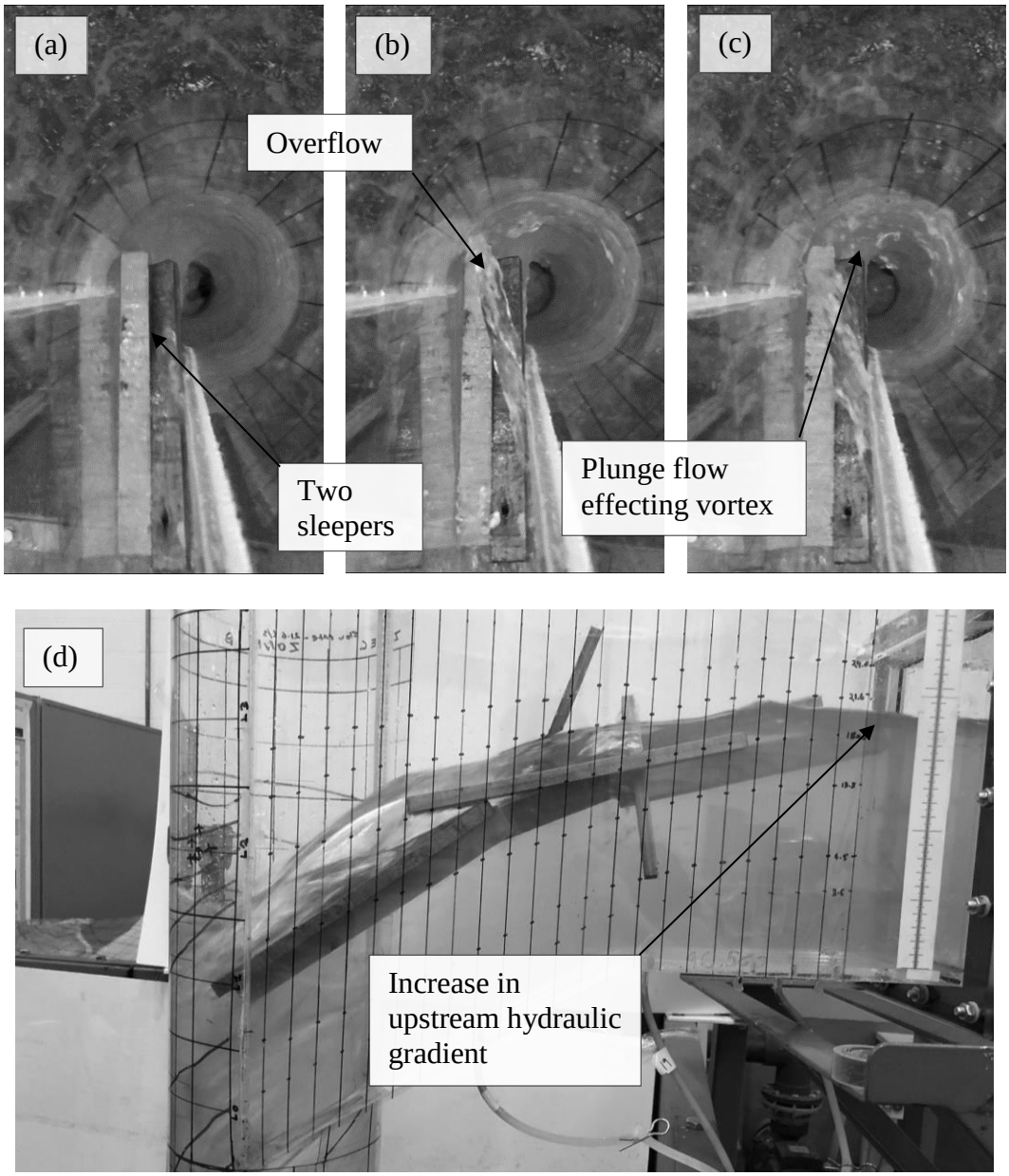

Figure 18. (a), (b), (c) debris jamming mechanisms in the vortex generator approach channel resulting in (d) changes in the hydraulic gradient and a (c) plunge flow mechanisms in the drop shaft

Discussion

Hydrodynamics

In the previous sections, a range of physical and numerical observations have been presented for hydrodynamic effects in a tangential inlet vortex drop shaft having implications on the structural integrity of the hydraulic structure. It is possible to infer from these observations that the fluid dynamics in the structure change rapidly as the flow progresses from the vortex generator to the downstream shaft. Essentially, this rapid and somewhat severe change in flow behaviour can simply be described by the transition of a linear flow in, for example the upstream sewer culverts and channels, to the rotational and largely axisymmetric flow in the downstream drop shaft. As was first observed in the physical and numerical observations of the air core at the vortex generator region, the conveyance of flow down the ramp combined with local acceleration at the inlet results in the generation of substantial kinetic energy in the inlet jet which is to subsequently change direction at the tangential inlet. The result is the generation of a forced vortex which causes the free-surface to jump and spread the flow tangentially around the periphery of the drop shaft. This develops a highly asymmetric free-surface and velocity distribution which is presented in Figures 10 and 11. The change of momentum, due to a change of the fluids direction results in the generation of a reaction force on the drop shaft liner in this region which is to be restrained during safe operation. The pressure on the fluid liner in this region is further intensified by the generation of a centrifugal force $a_c = {v_\theta}^2/r$ due to high tangential velocities localised over a small inlet radius r. This inlet flow mechanisms thus explains the peak pressure distributions observed for a distance of $Z/D = 5$ downstream of the vortex generator as is presented in Figure 13 which intensifies as the flowrate and inlet circulation increases. Downstream of this region, the free-surface and velocity distribution in the annular jet becomes more evenly distributed

as a result of the energy dissipation process. However, a single steady asymmetric wave exists for the extent of the drop shaft manifesting as a helical free-surface wave.

As is summarised in Figure 19 and, despite the minor asymmetry in the flow, it can be assumed that the stream line angle α at any circumferential position θ is constant for axial heights downstream of Z/D =5. Thus the streamline angle can be approximated for this region by:

$$\alpha = Tan^{-1}\frac{v_z}{v_\theta} \tag{1}$$

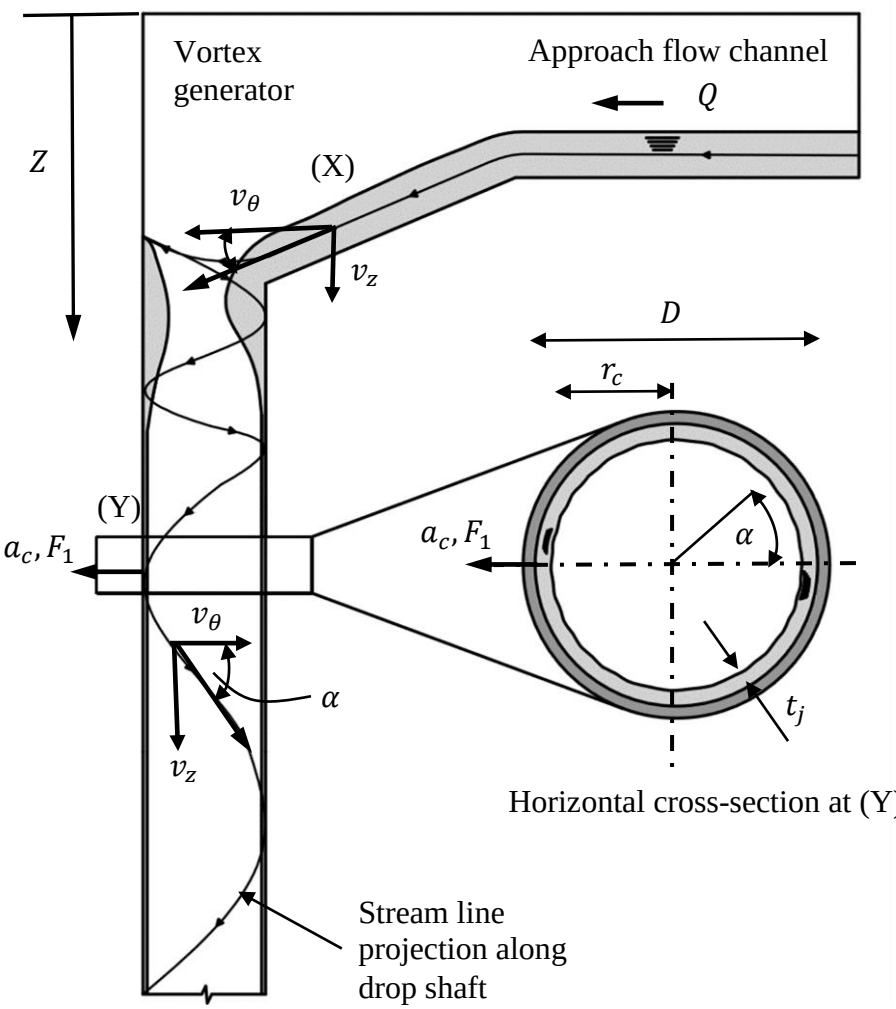

Figure 19. Hydraulic analysis of flow in the vortex drop shaft as a result of initial circulation conditions in the vortex generator

For an axisymmetric annular flow, it can also be assumed that the axial velocity is constant over the annular cross section at say (1), thus:

$$v_{z(1)} = \frac{Q}{\pi(\frac{D^2}{4} - {r_c}^2)} \quad (2)$$

Therefore, at any Z depth in the drop shaft, it is then possible to resolve the tangential velocity in the annular jet by:

$$v_{\theta(1)} = \frac{Q}{\pi(\frac{D^2}{4} - {r_c}^2)Tan\alpha} \quad (3)$$

or the centrifugal force applied on the walls of the drop shaft by:

$$a_{c(1)} = \frac{\left(\frac{Q}{\pi(\frac{D^2}{4} - {r_c}^2)Tan\alpha}\right)^2}{r} \quad (4)$$

Thus, if the nature of the streamline behaviour throughout the vertical extent of the drop shaft is known (i.e. $d\alpha/dZ$), and the annular jet thickness is $t_j = D/2 - r_c$ is assumed to be constant as is a good approximation for $Z \geq Z/D = 5$. In this study, the streamline trajectories $d\alpha/dZ$ were resolved for the initial portion of the drop shaft. A good relationship between α and Z was resolved for all data points (see Figure 20) and was expressed:

$$\alpha = 32.94Z^{-0.735} + 100 \quad (5)$$

where a power curve was used as a best fit line assuming that the final streamline exiting the drop shaft had an angle of 90˚ which is typical in the exit of a vortex drop shaft structure (Weiss et al, 2010). Verticality of the streamline in this region can also be ascertained from the numerical modelling results where the tangential velocity at the exit approaches 0 m/s (see Figure 12) Provided this best fit curve provides a good approximation of the streamline angles for $Z \geq 1.0$, its equation can be combined with Eq(4) can be used to resolve the axial distribution of force and pressure along the drop shaft liner can be resolved for design purposes. Thus, by only physically modelling a

small portion of the drop shaft (26 % in this case) it is possible to resolve crucial design information without the requirements of consulting costly physical modelling facilities (permitting sufficient vertical space for physical model builds) or numerical modelling software.

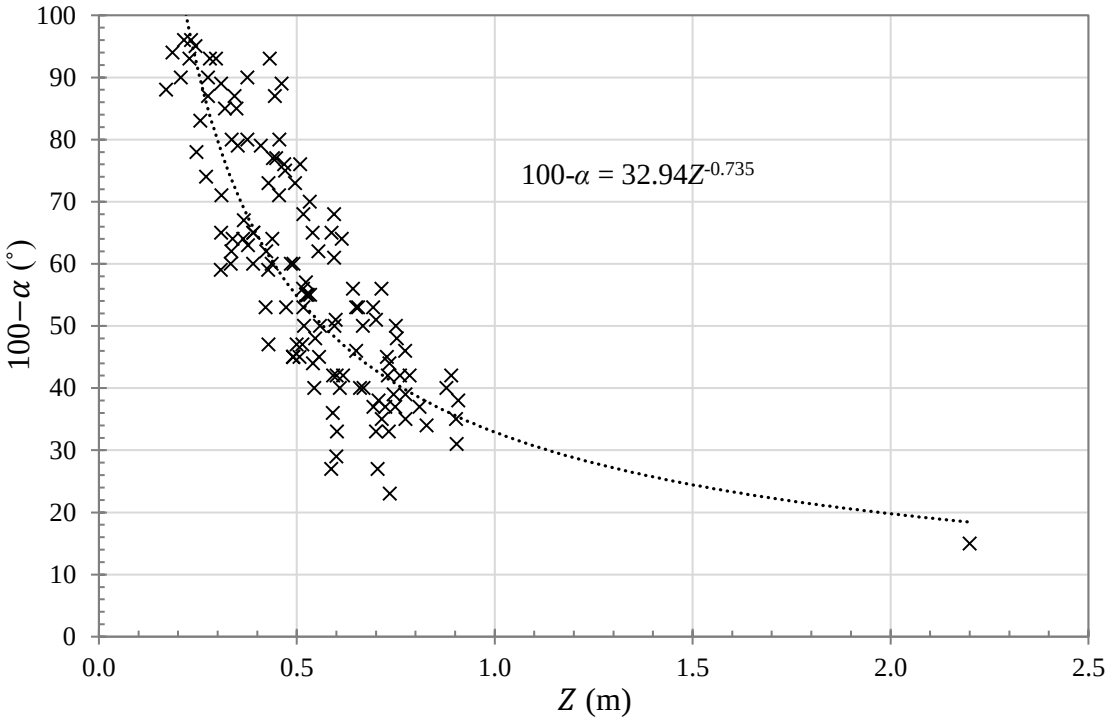

Figure 20. Relationship between α and Z for all data obtained in the stream line analysis. Data point at 2.2 was assumed to provide a strong relationship between α and Z

Mechanisms Driving Liner Degradation – Impact, Erosion and Abrasion

Apart from corrosion, the liner material in a drop shaft is subject to degradation due to several hydrodynamic mechanisms, namely impact, erosion and abrasion. Physical model studies on debris impact were presented previously using woody debris such as railway sleepers. A localised region prone to impact was identified in the vortex generator again due to the severe change of fluid acceleration and direction in the tangential inlet. Debris accelerations were resolved for each discharge and were found to be of the order of 3.5

530 m/s^2 driven by gravitational acceleration on the ramp and local fluid acceleration both
531 horizontally and axially. The impact force of the debris was calculated to be of the order
532 of 0.26 N in the model (260 N in the prototype). Appearing to be small, if the debris
533 impacts the liner at its sharp edge, the force applied over a small localised area may
534 manifest as a high puncturing stress which may breach the surface of the liner. Given that
535 the point of impact of the debris in the experiments was localised, continuous impact due
536 to debris laden flows is an item which should be considered when designing and choosing
537 a suitable material for a drop shaft liner. It must also be noted that this issue would only
538 be prominent in the vortex generator region where in the remaining drop shaft, the flow
539 conditions are largely axial.

540 With knowledge of the streamline angles and hence the tangential and axial
541 velocities in the vicinity of the liner surface, it is also possible to draw conclusions on the
542 wearing effects of erosion and abrasion on the liner given that such flows generally
543 contain large solids concentrations. Abrasion is a wear phenomenon involving
544 progressive material loss due to hard particles forced against and moving along a solid
545 surface (Auel et al., 2015). Particles are transported in sliding, rolling or saltation motion
546 depending on the flow conditions causing grinding, rolling or saltating impact stress on a
547 liner material. According to Sklar and Dietrich (2001), the governing process causing
548 abrasion is saltation, whereas sliding and rolling do not cause significant wear. Regarding
549 the vortex chamber flow dynamics, saltation would be expected to be largely present
550 again at the entrance to the vortex generator due to the change of direction of flow. Sliding
551 and rolling would dominate the remainder of the drop shaft where the radial velocity is
552 negligible. A number of models exist to predict the abrasion rate of materials due to the
553 abovementioned mechanisms (Ishibashi, 1983; Sklar and Dietrich, 2004; Auel, 2015)
554 wherein the parameters required can be derived from the hydrodynamic variables

555 explored in this study (impact angle, stream velocity components, suspended solids
556 concentration, centrifugal forces, wall pressures etc.) together with material properties.
557 Although not explored further in this study, this topic wold nonetheless be a fruitful future
558 investigation.

559 **Critical Helical Height Hypothesis**

560 From the previous discussion, it is clear that the vortex drop shaft is most prone to
561 structural damage or degradation in the vortex generator region for an axial distance
562 downstream of the generator (found in this study to be limited to $5D$ downstream from
563 the vortex generator). This is due to (1) reaction forces generated at the inlet, (2)
564 centrifugal forces resulting from a circulation dominated flow producing high wall
565 pressures, (3) large pressure fluctuations which, combined with high local fluid velocities
566 may lead to the onset of cavitation, (4) localised debris impact locations and (5) saltation
567 abrasion mechanisms at the vortex generator inlet. All the previous mechanisms can be
568 seen to be attributed to rotational flow hydrodynamics which dominates the first section
569 of the drop shaft. However, it is also evident from the axial distributions of velocity and
570 pressure that the centrifugal forces diminish in a streamwise direction downstream. This
571 can be further revealed through Eq(3) which shows that as the streamline angle
572 approaches 90 degrees, the tangential velocity tends towards 0. Therefore, it is here
573 proposed that there must exist some critical height where, depending on the material
574 properties of the drop shaft liner, the mechanisms driving structural damage or wear in
575 the drop shaft are minimal such that a change of material from a high structural design
576 capacity to a lower one could be considered to save in costs. This proposal has significant
577 implications on potential cost savings in heavy infrastructure projects requiring large drop
578 shaft structures. For example, rather than employing a stainless-steel drop shaft liner for
579 the full length of drop, if an axial location Z in the drop can be identified where the use

of stainless-steel material is excessive from a material strength perspective, a changeover of material to a lower cost material can be justified to carry the flow to the bottom of the drop shaft structure.

Conclusions

In this study, a comprehensive investigation into the hydrodynamic mechanisms affecting the structural performance and maintenance of vortex drops shaft structures is undertaken using physical and numerical models. Physical model studies for a 1/10 scaled model of a tangential inlet vortex drop shaft are undertaken to investigate free-surface characteristics, streamline characteristics, pressure fluctuations, debris impact and debris blocking mechanisms. The data was used to validate a multiphase numerical model of the flow to reveal further three-dimensional velocity and pressure distributions along the full length of drop structure. The key conclusions from the research are as follows:

- The research identified five primary hydrodynamic mechanisms that affect the structural integrity of drop shafts: (1) the reaction forces generated at the inlet, (2) the centrifugal forces resulting from a circulation dominated flow producing high wall pressures, (3) the large pressure fluctuations which, combined with high local fluid velocities may lead to the onset of cavitation, (4) the localised debris impact locations and (5) the saltation abrasion mechanisms at the vortex generator inlet all instigated by centrifugal forces which dominate this region of the drop shaft. To the authors' knowledge, this is the first study to explicitly identify these mechanisms and they are therefore a key novelty of the research. We recommend that they should set the basis for progressing further fluid structure interaction studies on vortex drop shaft structures.

- The identified hydrodynamic mechanisms are attributed to the vortex generator and a

distance of drop shaft downstream, below which the centrifugal forces diminish lowering the risk to potential structural damage. A relationship to model the reduction in centrifugal forces on the drop shaft liner and identify the critical helical height for the shaft was developed. This requires only a brief streamline investigation to be carried out on the vortex generator section of the overall drop structure. In this study the critical height was found to be five times the shaft diameter (*5D*).

Due to a lowered risk of potential damage below the critical height the authors propose that there is scope for significant cost savings in the design and construction of vortex drop shafts by substituting costly, high strength materials for lower cost materials for the portion of the shaft below 5D. The location of material changeover could be identified by analysing the streamline angles and air core diameters for various flow conditions in a short section of the vortex generator and drop to predict the centrifugal force along the full extent of the drop.

Acknowledgements

The authors of this work would like to thank Ward and Burke Construction Ltd for their support when compiling this article. The authors would further like to express gratitude to Edward Kilcullen and Dermot Mc Dermott for their assistance during physical modelling investigations.

Notation

Γ	= circulation	($m^2 s^{-1}$)	H	= chamber height	(m)
Γ_∞	= bulk circulation	($m^2 s^{-1}$)	θ,r,z	= coordinates	(-)
Q	= flow rate	($m^3 s^{-1}$)	t	= time	(s)
v_θ	= tangential velocity	($m s^{-1}$)	σ	= surface tension coefficient	($N m^{-1}$)
v_z	= axial velocity	($m s^{-1}$)	g	= gravitational coefficient	($m s^{-2}$)
v_r	= radial velocity	($m s^{-1}$)	ν	= kinematic viscosity	($m^2 s^{-1}$)
p	= pressure	($N m^{-2}$)	α	= Streamline angle	(°)
D	= drop shaft diameter	(m)	F	= outlet Froude number	(-)
h	= approach flow depth	(m)	R_e	= Reynolds number	(-)
r	= radius	(m)	W_e	= weber number	(-)
r_{in}	= inlet radius	(m)	S	= ramp of slope	(°)

B	= inlet channel width	(m)	λ	= Froude similitude scaling factor	(-)
b	= throat width	(m)	$L_{m,p}$	= Length (model, prototype)	(m)
a_c	= Centrifugal force	(N)	D	= Shaft diameter	(m)
h	= Flow depth	(m)	Z	= Vertical height	(m)
t_j	= annular jet thickness	(m)	θ	= Circumferential position	(°)
V	= resulting velocity vector at inlet	(m s^{-1})	r_c	= Drop shaft radius	(m)
L	= Length	(m)	F	= Force	(N)
T	= Time	(s)	P	= Pressure	(N m^{-2})
A	= Acceleration	(m/s^2)	M	= Mass	(kg)

623

624

References

Ackers, P. & Crump, E.S., (1960). The vortex drop. *Proceedings of the Institution of Civil Engineers*, *16(4)*, pp.433-442.

Anderson, A.G. & Dahlin, W., (1975). *Model studies of drop shafts for the tunnel and reservoir plan*. University of Minnesota, St Anthony's Falls Research Laboratory, Minneapolis, Minnesota, United States of America

Anderson, S.H. (1961). *Model studies of storm-sewer drop shafts.* University of Minnesota, St Anthony's Falls Research Laboratory, Minneapolis, Minnesota, United States of America

Auel, C., Albayrak, I., Sumi, T. & Boes, R.M. (2015). Saltation-abrasion model for hydraulic structures. *In Proc. Int. Workshop on Sediment Bypass Tunnels*. pp. 101-121.

Auel, C. (2014). *Flow characteristics, particle motion and invert abrasion in sediment bypass tunnels*. Doctoral dissertation, ETH Zurich, Zurich, Switzerland.

Chen, H.Y., Xu, W.L., Deng, J., Niu, Z.P., Liu, S.J. & Wang, W. (2010). Theoretical and experimental studies of hydraulic characteristics of discharge tunnel with vortex drop. *Journal of Hydrodynamics*, *22(4)*, pp.582-589.

Drioli, C. (1947). Su un particolare tipo di imbocco per pozzi di scarico. *L'Energia Elettrica, 24(10)*, 447-452.

Dong, X. & Gao, J. (1995). *Report on model study of retrofitting a diversion tunnel into a vortex drop shaft spillway in Shapai PowerStation*. IWHR Research Rep., China Institute of Water Resources and Hydropower Research, China (in Chinese).

Dahlin, W.Q. & Wetzel, J.M. (1985). *Phoenix-Casa Grande Highway Storm water Interceptor Drop Structures Model Studies.* University of Minnesota, St Anthony's Falls Research Laboratory, Minneapolis, Minnesota, United States of America

Faram, M.G. & Harwood, R. (2000). CFD for the water industry; the role of CFD as a tool for the development of wastewater treatment systems. *In Fluent users' seminar*.

Hager, W.H. (1985). Head-discharge relation for vortex shaft. *Journal of hydraulic engineering*, *111(6)*, pp.1015-1020.

Hager, W. H. (1990) Vortex drop inlet for supercritical approaching flow. *Journal of Hydraulic Engineering, 116(8)*, pp. 1048-1054.

658 Hirt, C.W. & Nichols, B.D. (1981). Volume of fluid (VOF) method for the dynamics of
659 free boundaries. *Journal of computational physics*, *39*(1), pp.201-225.
660 Ishibashi, T. (1983). Hydraulic study on protection for erosion of sediment flush
661 equipments of dams. *Civil Society Proc. 334(6)*, 103–112 (in Japanese).
662 Jain, A. K., Garde, R. J. & Ranga Raju, K. G. (1978). Vortex formation at vertical pipe
663 intakes. *Journal of the Hydraulics Division, 104(10),* pp. 1429-1445.
664 Jain, S. C. & Kennedy, J. F. (1983) *Vortex-flow drop structures for the Milwaukee*
665 *Metropolitan Sewerage District inline storage system*. Iowa Institute of Hydraulic
666 Research, the University of Iowa, Iowa, United States of America
667 Jain, S. C. (1984). Tangential vortex-inlet. *Journal of Hydraulic Engineering, 110(12),*
668 pp. 1693-1699.
669 Jain, S. C., & Ettema, R. (1987). *Vortex-flow intakes*. IAHR Hydraulic Structures Design
670 Manual, Vol. 1, A. A. Balkema, Rotterdam, The Netherlands.
671 Jeanpierre, D. & Lachal, A. (1966). Dissipation d'énergie dans un puits à vortex. *La*
672 *Houille Blanche, (7)*, pp. 823-832
673 Kim, S.Y., Kim, J.S. and Yoon, S.E., (2014). Analysis of Discharge Capacity for Intake
674 Structure at Deep Underground Storm Water Tunnel Using Fluent Model. *Journal*
675 *of Korean Society of Hazard Mitigation, 14(2),* pp.255-265.
676 *Kinovea* (Version 0.8.15) [Software program]. Available at www.kinovea.org (Accessed
677 15 October 2018)
678 Schultz, N., Munsey, F. & Parente, M., (2004). Deep Tunnels for Sewage Storage and
679 Conveyance: Lessons and Opportunities. *Proceedings of the Water Environment*
680 *Federation*, 2004(10), pp.643-669.
681 Plant, J. & Crawford, D. (2016). Pushing The Limits Of Tangential Vortex Intakes: Is
682 Higher Capacity And Flow Measurement Possible In A Smaller Footprint?.
683 *Proceedings of the Water Environment Federation*, 2016(12), pp.4108-4136.
684 Tai, R., Chan, A. & Seit, R. (2009) Planning of deep sewage tunnels in Hong Kong. *In*
685 *ITA-AITES World Tunnel Congress Open Session*
686 Kellenberger, M. H. (1988). *Wirbelfallschächte in der Kanalisationstechnik*.
687 Mitteilungen der Versuchsanstalt fur Wasserbau, Hydrologie und Glaziologie an
688 der Eidgenossischen Technischen Hochschule Zurich, (98), pp. 1-367.
689 Laushey, L. M. (1953). Studies show Pittsburgh how to drop sewage 90ft vertically to
690 tunnel interceptors. *Engineering News Records*.

691 Motzet, K. M. and Valentin, F. (2002). Efficiency of a vortex chamber with horizontal
692 bottom under supercritical flow. *IX International Conference on Urban Drainag*e.
693 Mulligan, S., Creedon, L., Casserly, J. and Sherlock, R. (2018a). An improved model for
694 the tangential velocity distribution in strong free-surface vortices: an experimental
695 and theoretical study. *Journal of Hydraulic Research*. pp.1-14.
696 Mulligan, S., Bonfils, T., O'Neill, C., Gonzalez, B., Carty, A., Clifford, E., and Nash, S.
697 (2018b). Multiphase numerical modelling of tangential inlet vortex drop shaft
698 structures. In *Civil Engineering Research in Ireland 2018: conference*
699 *proceedings.* Civil Engineering Research Association of Ireland (CERAI). 29th
700 to the 30th of August, 2018 University College Dublin (UCD), Dublin, Ireland
701 Mulligan, S., Casserly, J. & Sherlock, R. (2016). Effects of geometry on strong free-
702 surface vortices in subcritical approach flows. *Journal of Hydraulic Engineering*,
703 *142(11),* p.04016051.
704 Mulligan, S., (2015). *Experimental and numerical analysis of three-dimensional free-*
705 *surface turbulent vortex flows with strong circulation*. Doctoral dissertation.
706 Institute of Technology, Sligo.
707 Quick, M.C. (1990). Analysis of spiral vortex and vertical slot vortex drop shafts. *Journal*
708 *of Hydraulic Engineering*, *116(3)*, pp.309-325.
709 Rhee, D.S., Park, Y.S. & Park, I. (2018). Effects of the bottom slope and guiding wall
710 length on the performance of a vortex drop inlet. *Water Science and Technology*,
711 *78(6)*, pp.1287-1295.
712 Škerlavaj, A., Škerget, L., Ravnik, J. and Lipej, A. (2014). Predicting Free-Surface
713 Vortices with Single-Phase Simulations. *Engineering Applications of*
714 *Computational Fluid Mechanics*, *8(2)*, pp. 193-210.
715 Stayton, P. (2017). How to Drop Two Stories without Breaking St*ff - A Sewer Story of
716 Energy Dissipation, *Idaho Operators Conference,* Moscow IDPacific Northwest
717 Clean Water Association, May 23, 2017
718 Sklar, L.S. & Dietrich, W.E. (2001). Sediment and rock strength controls on river incision
719 into bedrock. *Geology*, *29*(12), pp.1087-1090.
720 Sklar, L.S. & Dietrich, W.E. (2004). A mechanistic model for river incision into bedrock
721 by saltating bed load. *Water Resources Research*, *40*(6).
722 UK Water Projects. (2015). Charlton Hayes Interceptor Sewer & Drop Shaft.
723 www.waterprojectsonline.com

724 Vischer, D.L. & Hager, W.H. (1995). *Energy dissipators, hydraulic structures design*
725 *manual.* IAHR, Balkema, Rotterdam, Netherlands
726 Williamson, S. (2001). Drop structure design for wastewater and storm water collection
727 systems. *1998 William Barclay Parsons Fellowship Parsons Brinckerhoff*
728 *Monograph 14*. Parsons Brinckerhoff.
729 Weiss, G., Brombach, H. & Hohl, E., (2010). Hydraulic model tests on a storm water
730 vortex drop shaft: Verification of special conditions. *Novatech, 7th International*
731 *Conference on Sustainable Techniques and Strategies for Urban Water*
732 *Management 2010.* Eurexpo - Espace Alto - Convention & Exhibition Center
733 Avenue Louis Blériot in Chassieu, Lyon, France.
734 Yu, D. & Lee, J.H. (2009). Hydraulics of tangential vortex intake for urban
735 drainage. *Journal of hydraulic engineering*, *135*(3), pp.164-174.
736 Zhao, C.H., Zhu, D.Z., Sun, S.K. & Liu, Z.P. (2006). Experimental study of flow in a
737 vortex drop shaft. *Journal of Hydraulic Engineering*, *132*(1), pp.61-68.
738 Zielinski, P.B. & Villemonte (1968). Effect of viscosity on vortex orifice flow. *Journal*
739 *of the Hydraulics Division, 94(3)*, pp.745-752.